UNIVERSITY OF TARTU

Faculty of Science and Technology

Institute of Bioengineering

Yelyzaveta Gushchyna

Establishing Phosphorylated Human Protein Kinase N3 Generation via PDPK1 Co-expression in Sf9 cells

Master's Thesis (30 ECTS)

Curriculum Bioengineering

Supervisor(s):

PhD Santa Veikšina

PhD Sergei Kopantšuk

PhD Kaido Viht

Tartu 2026

Establishing Phosphorylated Human Protein Kinase N3 Generation via PDPK1 Co-expression in Sf9 cells

Abstract

Protein Kinase N3 (PKN3) is an AGC family serine/threonine kinase implicated in cancer due to its elevated expression in tumour cells. Its activation requires phosphorylation (Thr718) and regulation by upstream factors, notably by phosphoinositide-dependent kinase 1 (PDPK1), which increases the amount of active PKN3. This work utilises the MultiBac baculovirus system to co-express PKN3 and PDPK1 in Sf9 cells, enabling production of phosphorylated PKN3. The protein is purified via Strep-tag affinity chromatography using Strep-Tactin. Furthermore, immobilisation of PKN3 on magnetic beads is explored to develop fluorescence-based assays, providing a platform for future high-throughput screening of PKN3 inhibitors.

Keywords

PKN3, PDPK1, phosphorylation, baculovirus expression system, protein co-expression, purification, immobilisation, magnetic beads, fluorescence microscopy

CERCS: P310 Proteins, enzymology; B230 Microbiology, bacteriology, virology, mycology

Institute name: Institute of Chemistry

Research group: Bioorganic Chemistry Chair

Inimese proteiinkinaasi N3 fosforüülitud vormi tootmise arendamine Sf9 putukarakkudes PDPK1 koosekspressiooni abil

Lühikokkuvõte

Proteiinkinaas N3 (PKN3) on AGC perekonda kuuluv seriin/treoniinkinaas, mis on seotud vähiga oma suurenenud ekspressiooni tõttu kasvajarakkudes. Selle aktivatsioon nõuab fosforüülimist (Thr718) ning regulatsiooni ülesreguleerivate faktorite poolt, millest oluline on fosfoinositiidsõltuv kinaas 1 (PDPK1), mis suurendab aktiivse PKN3 hulka. Käesolevas töös kasutatakse MultiBac bakuloviiruse süsteemi PKN3 ja PDPK1 ko-ekspressiooniks Sf9 rakkudes, võimaldades fosforüülitud PKN3 tootmist. Valk puhastatakse Strep-märgise abil Strep-Tactin afiinsuskromatograafia teel. Fluorestsentsmikroskoopia abil analüüsitakse magnetosakestele immobiliseeritud PKN3, millel põhinevat lähenemist arendatakse PKN3 inhibiitorite skriinimiseks.

Võtmesõnad:

PKN3, PDPK1, fosforüülimine, bakuloviiruse ekspressioonisüsteem, valkude ko-ekspressioon, puhastamine, immobiliseerimine, magnetosakesed, fluorestsentsmikroskoopia

CERCS: P310 Proteiinid, ensümoloogia; B230 Mikrobioloogia, bakterioloogia, viroloogia, mükoloogia

TABLE OF CONTENTS

TERMS, ABBREVIATIONS AND NOTATIONS

AGC – family of Serine/Threonine protein kinases defined by the similarity of the catalytic domains of the Protein Kinase A, Protein Kinase G and Protein Kinase C

AP – alkaline phosphatase

APS – Ammonium Peroxodisulphate

hPKN3 – Human Protein Kinase N3

hPKN3×PDPK1 – Human Protein Kinase N3 co-expressed with Phosphoinositide-dependent protein kinase

ICSE – Image-based Cell-Size Estimation

LDS – Lithium Dodecyl Sulfate

MOI – Multiplicity of Infection

PDPK1 – Phosphoinositide-dependent protein kinase 1

PES – Polyethersulfone

PI3K – Phosphoinositide 3-kinase

PK – Protein Kinase

PKC – Protein Kinase C

PKN – Protein Kinase N

PKN3 – Protein Kinase N3

PVDF – Polyvinylidene difluoride

rBV1 – Recombinant Baculovirus that expresses Strep-tagged human Protein Kinase N3

rBV2 – Recombinant Baculovirus that expresses Strep-tagged human Protein Kinase N3 and Phosphoinositide-dependent protein kinase 1

rBV3/rBV-empty – Control baculovirus derived from the empty construct

Sf9 – *Spodoptera frugiperda* 9 insect cell line

TEMED – Tetramethylethylenediamine

VSVG – Vesicular Stomatitis Virus Glycoprotein G

INTRODUCTION

Protein Kinase N3 (PKN3) is a serine/threonine protein kinase (PK) that belongs to the AGC kinase family, which includes Protein Kinase A, G, and C, and is a member of the protein kinase N (PKN) subfamily. While Protein kinase N1 (PKN1) and protein kinase N2 (PKN2) are broadly expressed, PKN3 expression is elevated in cancer cell lines, making it a promising target for anticancer drug development. PKN3 activation depends on the phosphorylation of the conserved threonine residue at position 718, as well as interaction with upstream activators, such as Rho-family GTPases. In addition, phosphoinositide-dependent kinase 1 (PDPK1) is a master regulator of the AGC kinases that phosphorylates and activates proteins of the AGC family. The catalytic activity of PKN3 is enhanced when expressed with PDPK1.

To study activated human PKN3 (hPKN3), an expression system capable of introducing eukaryotic post-translational modifications is required. Bacterial expression systems are widely used for recombinant protein production, but they are not suitable for producing active hPKN3 since they do not provide the eukaryotic post-translational modifications required for proper hPKN3 regulation. Mammalian expression systems can provide post-translational modifications, but they are more time-consuming and more expensive. The MultiBac baculovirus system is a suitable alternative for recombinant protein production, as it allows a simultaneous co-expression of hPKN3 and PDPK1 in Sf9 insect cells.

Recombinant hPKN3 can be purified by affinity chromatography using a Strep-tag, which binds specifically to Strep-Tactin and enables the isolation of active hPKN3. However, the alternative method of studying PKN3 activity is explored by immobilising hPKN3 on Strep-Tactin coated magnetic beads, by combining bead-based immobilisation with fluorescence-based readouts, it is possible to develop sensitive and scalable assays to assess PKN3 activity and its inhibition. Therefore, the establishment of a robust method for producing, purifying, and immobilising active PKN3 introduces an important step towards the development of high-throughput assays for the identification of PKN3 inhibitors.

1 LITERATURE REVIEW

1.1 Protein Kinases

PKs belong to the class of enzymes that catalyze one of the most widespread post-translational modifications – protein phosphorylation. Phosphorylation can modify protein-protein interactions, subcellular localisation, and protein conformation. Numerous cellular processes, such as the cell cycle, growth and apoptosis, are regulated by PKs (Wang et al., 2025). Approximately 30% of human proteins are regulated through kinase activity (Ardito et al., 2017). Many cellular activities, including kinase cascade activation, gene transcription, membrane transport, and metabolic pathways, are regulated by phosphorylation by PKs in response to extracellular signals, enabling cells to switch diverse functions on or off (L. N. Johnson & Lewis, 2001). PKs play a significant role in various pathologies, such as cancer and autoimmune disorders (Roskoski, 2026).

The human kinome comprises 518 PKs, which are classified based on the amino acid residues they phosphorylate. Among them, more than 300 are serine/threonine PKs, which phosphorylate serine and threonine residues. Other PKs phosphorylate tyrosine residues, while dual-specificity kinases can phosphorylate both serine/threonine and tyrosine residues. PKs can be activated through autophosphorylation or by proteins that can activate or inhibit their activity (Ardito et al., 2017; J. L. Johnson et al., 2023).

Conventionally, the catalytic subunit of PKs consists of a domain of approximately 250 amino acids comprising a small N-terminal lobe formed by β-sheets and a larger C-terminal lobe formed by α-helices. There is a cleft between the two lobes where ATP binds, positioning its triphosphate chain outward and its adenosine moiety in a hydrophobic pocket. When the substrate is recognized by a PK, it is positioned within the cleft next to ATP. Conserved amino acids in the catalytic domain of the PK then mediate the transfer of the terminal γ-phosphate of ATP to the hydroxyl group of tyrosine, threonine, or serine residues in the substrate (Ubersax & Ferrell Jr, 2007). Phosphoryl transfer is supported by Mg^{2+} ions, which are essential for ATP binding (Adams, 2001).

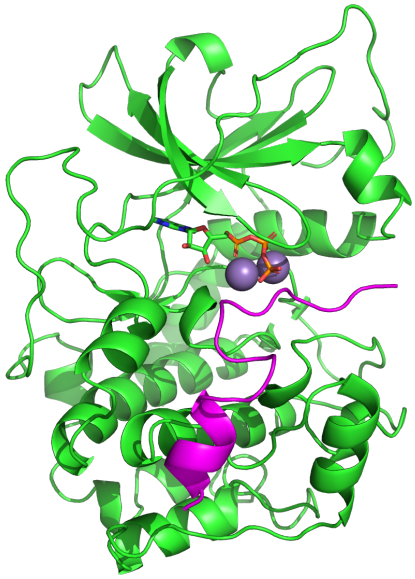

Figure 1. X-ray co-crystal structure of the catalytic subunit of cAMP-dependent protein kinase (PKA) complexed with MnATP and a peptide inhibitor (violet). The catalytic subunit of PKA (pdb: 1ATP) shares a conserved catalytic region with PKN3 (Jumper et al., 2021; Varadi et al., 2022; Zheng et al., 1993).

1.1.1 AGC Group of Protein Kinases

The AGC group is a subgroup of serine/threonine protein kinases defined by sequence similarity within their catalytic domain to protein kinase A, protein kinase G and protein kinase C. Activation of AGC kinases is associated with phosphorylation at conserved regulatory motifs, including the T-loop (activation loop) within the catalytic domain, as well as the hydrophobic motif and the turn motif located in the C-terminal non-catalytic region following the kinase domain (Garcia et al., 2012). PDPK1 is considered a master regulator of AGC kinases, activating and phosphorylating over 23 AGC kinases, including the protein kinase C (PKC) family (Pearce et al., 2010). The PKC superfamily includes PKC isoforms as well as PKC-related kinases such as PKN1, PKN2, and PKN3. PKC isozymes participate in signal transduction pathways triggered by various external stimuli, such as hormones and growth factors. PKC isozymes are involved in a range of diseases, including cardiovascular, neurological, and metabolic disorders, as well as multiple types of cancer. As a result, PKC isozymes are highly attractive therapeutic targets. One understudied group within this superfamily is the PKN kinase family (Kang, 2014).

1.1.1.1 PKN Family

PKNs belong to the AGC group of protein kinases. PKNs 1-3 are serine/threonine kinases that are part of the PKC-related kinase family (Leroux et al., 2018). PKNs have a molecular weight of approximately 100 kDa (Falk et al., 2014). PKNs function as effector proteins of Rho GTPases, small proteins that regulate cell motility and cytoskeletal dynamics; they bind to the N-terminal domain of PKN only in their activated, GTP-bound form, thereby promoting PKN activation and increasing its autophosphorylation rate (Watanabe et al., 1996). The PKN family regulates numerous processes, including cell cycle regulation, vesicular transport, receptor trafficking, and apoptosis (Collazos et al., 2011). While PKN1 and PKN2 are widely expressed, PKN3 is limited to muscle, liver and endothelial cells and shows elevated expression in multiple tumour cell lines, which makes it an attractive therapeutic target (Quétier et al., 2016).

1.1.1.1.1 PKN3

PKN3 is a serine/threonine protein kinase of the PKN family. PKN3 is involved in the regulation of malignant prostate cell growth downstream of activated phosphoinositide 3-kinase. It is known that PKN3 mRNA is highly expressed in a range of cancer cell lines; but shows limited expression in adult human tissues. This kinase is strongly associated with malignancy; it can act as a mediator of invasive prostate cancer cell growth downstream of the phosphoinositide 3-kinase (PI3K) pathway. PKN3 is regulated during the activation of PI3K signaling and can behave as an effector of the oncogenic PI3K signaling network (Figure 3) (Unsal-Kacmaz et al., 2012). Additionally, PKN3 can interact with p130 Cas (Crk-associated substrate) adaptor protein, which functions as a regulator of cancer cell growth. Together, PKN3 and p130 Cas are expressed in prostate adenocarcinoma and invasive breast cancer (Gemperle et al., 2019).

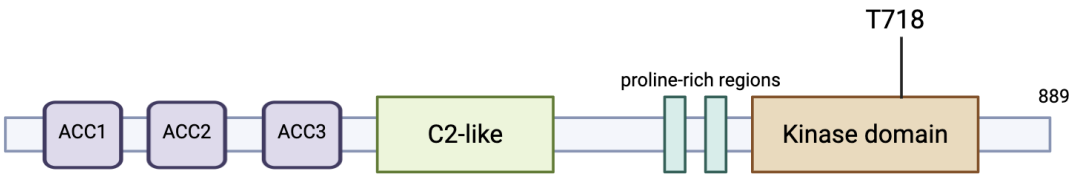

Figure 2. Domain organization of PKN3. PKN3 consists of three N-terminal domains (ACC1-3), C2-like domain and C-terminal serine/threonine kinase domain, two proline-rich regions and the Threonine 718 activation loop. The schematic was created based on (Sophocleous et al., 2021) (created with Biorender).

PKN3 is composed of five major domains (Figure 2): three N-terminal ACC domains (ACC1-3), a C2-like domain containing an autoinhibitory element, and C-terminal serine/threonine kinase domain containing the Thr718 activation-loop phosphorylation site. The ACC domains contain homologous segments enriched in charged residues and leucine zipper-like sequences. RhoA and RhoC GTPases specifically interact with the N-terminal region of PKN3 (Wang et al., 2025). The interaction between PKN3 and RhoC has been associated with aggressive tumour progression, and RhoC knockdown was demonstrated to block PKN3 overexpression, suggesting that PKN3-RhoC complex may contribute to the formation of aggressive tumours (Unsal-Kacmaz et al., 2012).Activation of PKN3 requires relief of autoinhibition within the C2-like domain and phosphorylation of Thr718 within the activation loop of the kinase domain (Wang et al., 2025).

The ATP-binding pocket of PKs is a highly suitable site for small-molecule inhibitors. Development of PK inhibitors remains a challenging task, as ATP-competitive inhibitors must target PK selectively as they compete with ATP for the ATP-binding pocket, which is strongly conserved and present in high millimolar concentration range inside the cells (Roskoski, 2026). Two inhibitors that are considered the best at suppressing PKN3 activity were identified: GSK902056A with apparent interaction constant (K_d^{app} of 1 nM) and GSK949675A (K_d^{app} of 2.5 nM), demonstrating high binding and specificity for PKN3 (Reinecke et al., 2024). Recent studies have identified highly selective PKN3 inhibitors: small-molecule 8-anilinoderivative of H-9 with dissociation constant (K_d) of 23 nM) and D-arginine-rich bisubstrate inhibitor ARC-2603 with K_d of

0.2 nM that were identified to have therapeutic potential of targeting PKN3 in future studies (Smorodina et al., 2026).

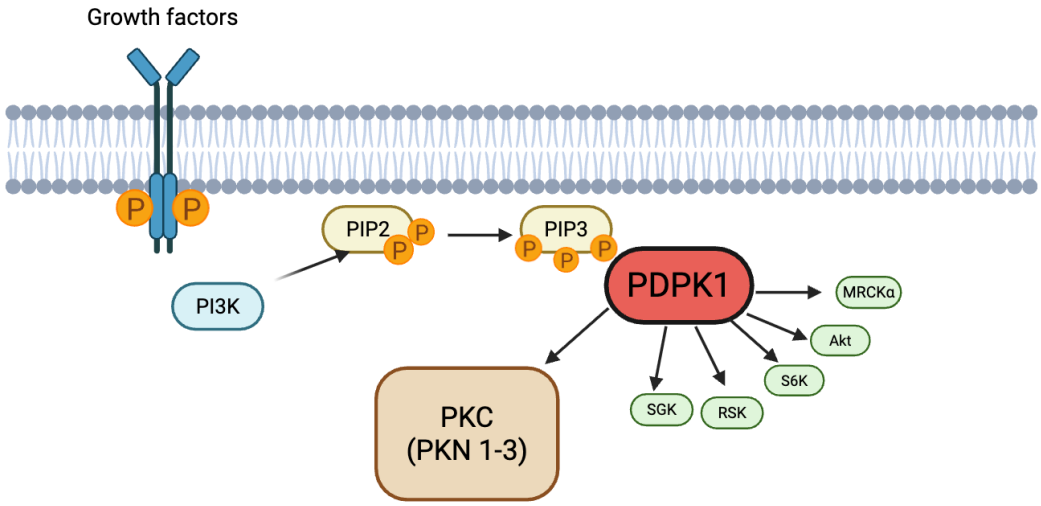

Figure 3.The phosphatidylinositol-3-kinase (PI3K)-3-phosphoinositide-dependent protein kinase-1 (PDPK1) pathway. PDPK1 acts downstream of PI3K as a key signaling mediator. Receptor-stimulated class I PI3Ks produce phosphatidylinositol (PIP3), which binds to the PDPK1 homology domain, leading to the activation of downstream targets, as shown in the scheme. PKN3, a PKC-related kinase, is also potentially activated by PDPK1 (Di Blasio et al., 2017) (created with Biorender).

Identifying the substrates of PKN3 is important for understanding how PKN3 regulates downstream signalling pathways. For investigating potential substrates of PKN3, it is essential to determine a phosphorylation consensus motif of PKN3 (Collazos et al., 2011). Both PKN1 and PKN3 favor the phosphorylation of Serine residues when the Arginine residue is located at -3, also PKN1/3 show specificity towards basic amino acids positioned downstream of the phosphorylation site and hydrophobic amino acids that are positioned at +1, consequently the proposed consensus motif for both PKN 1/3 is Lys-Arg-Arg-Lys-Pro-Ser-Phe-Arg-Asn-Pro (Shiga et al., 2010). Among the known substrates of PKN3 is ARHGAP18, which is phosphorylated by PKN3, promoting activation of the GAP domain (a conserved protein region that acts as a molecular switch) for RhoA GTPases (Dibus et al., 2020). Additionally, CLIP-170 (cytoplasmic linker protein of 170 kDa) and EGFR (epidermal growth factor receptor) were identified as substrates for PKN3 (Collazos et al., 2011).

1.1.1.2 PDPK1 (Phosphoinositide-dependent protein kinase)

Phosphoinositide-dependent protein kinase (PDK1, also known as PDPK1) is an upstream kinase that phosphorylates kinases of the AGC group at serine/threonine residues of their activation loop (Falasca & Fyffe, 2013). PDPK1 has two functional domains: the C-terminal PH domain and the N-terminal catalytic core. PDPK1 activity depends on phosphorylation of Ser241 within its activation loop. AGC kinase substrates bind to the PIF (PDPK1-interacting fragment) pocket of PDPK1 via their phosphorylated hydrophobic motif (N. Zheng et al., 2023).

1.1.1.2.1 Interaction Between PKNs and PDPK1

Activation of PKNs requires PDPK1-mediated phosphorylation of their activation loop and turn motif (Falk et al., 2014). The binding of Rho proteins to PKNs induces a conformational change that facilitates their interaction with PDPK1. PDPK1 phosphorylates PKN1 and PKN2 at conserved threonine residues located within their activation loops, resulting in the catalytic activation of PKN 1/2 (Unsal-Kacmaz et al., 2012). PKN1 and PKN2 are phosphorylated at Thr774 and Thr816, respectively depending on Rho-mediated activation (Flynn et al., 2000). When PKN3 is co-expressed with RhoA and RhoC, its catalytic activity is elevated, and even more enhanced when co-expressed with PDPK1. These findings suggest that PDPK1 increases PKN3 catalytic activity, particularly when it is in a complex with RhoC (Unsal-Kacmaz et al., 2012).

1.2 Introduction to Methods

1.2.1 Expression Systems

To study PKN3, it is important to select the most efficient expression system, as maintaining its phosphorylation state is a key objective (Slovakova & Bilkova, 2021). The prokaryotic expression system is commonly used for recombinant protein expression, since it allows easy scale-up, the ability to grow on inexpensive carbon sources, and a high growth rate. Unfortunately, the bacterial expression system does not support post-translational modifications, and often leads to inactive proteins and aberrant autophosphorylation, making this system unsuitable for PKN3 production (Sahdev et al.,

2007; Shrestha et al., 2012). Mammalian expression systems are generally considered the most suitable, as they provide essential post-translational modifications, ensure proper protein folding, and enable the production of large proteins. However, the insufficient yield and the cost of expression limit the practicality of mammalian expression systems. The expression in insect cells using the baculovirus expression system appeared to be an excellent approach for recombinant protein production, since it provides proper folding, post-translational modifications similar to those in mammalian cells, cost-effective production, and scalability (Kwiatkowska et al., 2025).

1.1.1.1 Baculovirus Expression System

The *Spodo ptera frugiperda* (Sf) insect cell system is widely used for recombinant protein expression. The Sf9 cell line is a clonal derivative of the Sf21 cell line derived from pupal ovarian tissue of fall armyworm *Spodoptera frugiperda.* Sf21 and Sf9 insect cell lines are both susceptible to baculovirus infection. However, the Sf9 line is often preferred because it is easier to maintain due to its higher growth rate. Sf9 cells are also more tolerant of high cell density, fluctuations in culture conditions, and shear stress. A drawback of Sf9 cells is their higher protease activity, which can compromise the stability of the expressed protein (Kwiatkowska et al., 2025)

For the production of recombinant proteins in Sf9 cells, the MultiBac expression system can be used. MultiBac is a baculovirus expression system that consists of synthetic DNA plasmids and an engineered baculovirus genome derived from *Autographa californica* nuclear polyhedrosis virus, designed for efficient multigene expression. The basic principle of MultiBac technology is that genes of interest are first inserted into acceptor and donor plasmids and assembled into a multigene construct via Cre-LoxP recombination. Next, a multigene acceptor-donor construct is transformed into *E. coli* cells containing the MultiBac baculoviral genome, where the Tn7 transposon system mediates integration of the expression cassette into the baculovirus genome. Subsequently, the MultiBac baculovirus genome in the form of bacmid is purified and can be utilised for insect cell transfection (Bieniossek et al., 2012). More detailed information about MultiBac generation can be found in the MultiBac™ Multi-Protein Expression in Insect Cells manual (Geneva Biotech, 2024).

1.1.2 Purification Strategies

When the recombinant protein is expressed in the desired expression system, the purification must be performed to eliminate contaminants and non-target proteins. Due to economic constraints, production of large amounts of purified protein is challenging, as production costs can range from 45% to 92% of the overall manufacturing cost of recombinant proteins. Consequently, choosing the optimal, cost-effective purification strategy is a major challenge in both academic and industrial settings (Saraswat et al., 2013). During purification, many factors can affect the process, including protein aggregation, protein inactivation, formation of inclusion bodies, incorrect folding, incorrect modifications, and low protein expression yield (Beygmoradi et al., 2023).

When isolating phosphorylated proteins, such as protein kinases, phosphorylation can drastically alter their behavior and should be considered when selecting the appropriate purification method. Ion exchange chromatography or chromatofocusing can be used, as phosphorylation shifts the isoelectric point of phosphoproteins, making them viable options when selecting a purification method. Another option is immobilised metal affinity chromatography, which can also be considered due to interactions between phosphate groups and metal ions. Additionally, immunoprecipitation can serve as an alternative, as phosphorylation alters the immunogenic properties of the proteins. However, affinity chromatography is often considered a highly effective technique for phosphoproteins as it selectively purifies phosphoproteins from the crude extract. Hence, the most effective strategy for obtaining highly pure phosphoproteins is to combine several purification methods (Schmidt et al., 2007).

1.1.2.1 Affinity Chromatography

Affinity chromatography enables the selective purification of target proteins from heterogeneous mixtures (Urh et al., 2009). The elution of the target protein depends on the reversible interaction between a ligand immobilised on a solid support or chromatographic matrix and the target protein. When recombinant proteins are expressed, it is necessary to select a specific, reversible ligand, which is usually achieved using fusion tags. Fusion tags are proteins or peptide sequences that enhance the expression of

the target protein in the host system and protect it against proteolytic degradation (Dutta & Bose, 2022). During elution, most non-specifically bound proteins are washed away, but the ligand immobilised on the matrix can also interact with other proteins in a non-specific manner, as host cells contain numerous proteins with diverse biophysical properties and abundances. Therefore, affinity chromatography can still present challenges when considered as a purification method (W. Zheng et al., 2015).

1.1.2.1.1 Strep-Tag

The Strep-tag is a short eight-amino acid peptide (Trp-Ser-His-Pro-Gln-Phe-Glu-Lys) that can be used as an affinity tag for the purification of recombinant proteins. It binds specifically and reversibly to streptavidin by occupying the biotin-binding pocket and thereby competing for streptavidin binding (Voss & Skerra, 1997). Streptavidin is a ~56 kDa homotetramer isolated from the bacterium *Streptomyces avidinii* that interacts with biotin molecules with $K_d \approx 10^{-14}$ M. Streptavidin is insensitive to high pH, enzymatic degradation, and denaturing agents, and that which makes it highly suitable for protein purification, serving as a robust matrix in its immobilised form during affinity purification (Dundas et al., 2013; W. Zheng et al., 2015). Usually, His-tags are used for purification of recombinant proteins, however the use of His-tags are less suitable for structurally unstable proteins. Therefore, Strep-tags can serve as an efficient alternative (Skerra & Schmidt, 1999).

.

2 THE AIMS OF THE THESIS

- To co-express recombinant hPKN3 and PDPK1 in Sf9 insect cells using the Baculovirus Expression system.
- To evaluate the phosphorylation status of hPKN3 upon co-expression with PDPK1.
- To evaluate the immobilisation and isolation of hPKN3 using MagStrep beads and to assess its potential for fluorescence-based microscopy assays.

2 EXPERIMENTAL PART

2.1 MATERIALS AND EQUIPMENT

Previously, three recombinant bacmids were generated at the University of Tartu, Bioorganic Chemistry Chair, using the MultiBac system. The constructs were assembled via Cre–lox recombination of acceptor (*ACE*) and donor (*D*) plasmids containing expression cassettes under dual-purpose insect/mammalian (*IM*) or insect-specific (*I*) promoters.

The following MultiBac constructs were used:

- *pIMACE*-hPKN3 × *pIDC*-VSVG – encoding Strep-tagged human PKN3 and VSVG
- *pIMACE*-hPKN3 × *pIDC*-VSVG × *pIMDK*-PDPK1 – encoding Strep-tagged human PKN3, VSVG, and PDPK1
- *pIMACE*-empty × *pIDC*-VSVG – empty backbone control

In these constructs, human PKN3 was fused to a Strep-tag to facilitate purification, VSVG was included to enable potential transduction of mammalian cells, and PDPK1 was used for co-expression studies. Bacmids generated from these MultiBac plasmids were used to produce recombinant baculoviruses in Sf9 cells, referred to as:

- rBV1 – expressing Strep-tagged hPKN3
- rBV2 – co-expressing Strep-tagged hPKN3 and PDPK1
- rBV3 (rBV-empty) – control virus derived from the empty construct

For simplicity, proteins expressed in Sf9 cells using rBV1 are referred to as hPKN3, whereas proteins obtained from co-expression using rBV2 are referred to as hPKN3×PDPK1. Samples generated using the control virus (rBV3) are referred to as empty control. A detailed scheme of construct generation is provided (Figure S1).

Sf9 cells (*Invitrogen*): insect cells isolated from pupal ovarian tissue of the fall armyworm *Spodoptera frugiperda*; EX-CELL® 420 Serum-free insect cell growth medium (*Sigma-Aldrich*); TC10™ Automated Cell Counter and counting slides (*BIO-*

RAD); 0.4% trypan blue solution (*Sigma*); Low protein binding PES (polyethersulfone) syringe filters with pore sizes of 0.22 µm and 0.45 µm (*Sartorius*); Serological and automatic pipettes with filter tips for cell culture handling; Laminar flow cabinets; The Cytation 5 imaging microplate reader was used with Gen6 software (*BioTek*); 24-well tissue culture-treated plates (*BioLite*); Lipofectamine™ LTX (with PLUS™ reagent) (*Invitrogen*);

Benchtop centrifuge 2-16KL (*Sigma*); 1% Triton X; 50 mM Tris-HCl, 150 mM NaCl; 10 mM glycerol-2-phosphate; 0.5 mM DTT; Phosphatase Inhibitor Cocktail (*Selleck chemicals*); Protease Inhibitor Cocktail (*Selleckchemicals*); DPBS (Dulbecco's Phosphate-Buffered Saline) with Ca^{2+} and Mg^{2+} (*Corning*).

Gravity flow column prepacked with Strep-Tactin® Superflow® high-capacity resin in 50% suspension in buffer, pH 8.0 (100 mM Tris/HCl, pH 8.0, 150 mM NaCl, 1 mM EDTA, 0.02% sodium azide) (*Iba Lifesciences*); Strep-Tactin®XT 4Flow® high capacity resin in 50% suspension buffer (*IBA Lifesciences*); 1× Buffer W (100 mM Tris/HCl pH 8.0, 150 mM NaCl, 1 mM EDTA) (*IBA Lifesciences*), 1× Buffer E (100 mM Tris/HC pH 8.0, 150 mM NaCl, 1 mM EDTA, 2.5 mM desthiobiotin) (*IBA Lifesciences*); 1× Buffer BXT (1 M Tris-HCl, 1.5 M NaCl, 10 mM EDTA, 500 mM biotin, pH 8) (*IBA Lifesciences*), 1× Buffer R (100 mM Tris/HCl, pH 8.0, 150 mM NaCl, 1 mM EDTA, 1 mM HABA) (*IBA Lifesciences*); MagStrep® StrepTactin®XT beads in 5% suspension (*IBA Lifesciences*); freshly prepared 100 mM NaOH (alternative regeneration for Strep-Tactin®XT 4Flow® high capacity resin); MagStrep® StrepTactin® XT beads in 5% suspension (IBA Lifesciences); magnetic separator (*ThermoFisher*); 1× Buffer W (100 mM Tris/HCl pH 8.0, 150 mM NaCl, 1 mM EDTA) (*IBA Lifesciences*); 1× Buffer BXT (1 M Tris-HCl, 1.5 M NaCl, 10 mM EDTA, 500 mM biotin, pH 8) (*IBA Lifesciences*);

Polyclonal rabbit anti-PKN3 antibody, maps to a region between residue 225 and 275 of human protein kinase N3 using the numbering given in entry NP_037487.2 (NBP-1-30102 Lot A1, *Bio-techne*); Anti-PKN3 (pT718) + PRK1 (pT774) + PKN2 (pT816) phospho antibody [EPR5671] - AB124709 (*Abcam*); custom-made at the University of Tartu, Bioorganic Chemistry Chair 48-well chamber with the functionalized coverslip attached and sealed with Topseal (*PerkinElmer*); Goat anti-Rabbit IgG (H+L) Secondary

Antibody, AP, (*ThermoFisher*); Secondary anti-rabbit antibody conjugated with Star Red (*Abberior*);

Vertical polyacrylamide gel protein electrophoresis system Mini-PROTEAN® Tetra System (*BIO-RAD*); Trans-Blot SD Semi-Dry Electrophoretic Transfer Cell protein blotting system (*BIO-RAD*); Thermomixer comfort (*Eppendorf*); Rocking shaker DRS-12 (*ELMI*); 30% acrylamide (*AppliChem*), 0.8% bis-acrylamide (*Bio-Rad*); Tris/SDS pH 8.8; Tris/SDS pH 6.8; 10 % Ammonium Peroxodisulphate (APS) (*AppliChem*), Tetramethylethylenediamine (TEMED) (*SIGMA Life Sciences*); NuPAGE™ Lithium Dodecyl Sulfate (LDS) Sample Buffer (4×) (contains Coomassie G250 and Phenol Red as tracking dyes) (*ThermoFisher*); Amersham™ Hybond P 0.45 PVDF (polyvinylidene difluoride) blotting membrane (*Cytiva*); blotting pad, 707 (filters) (*VWR*); Transfer buffer (50 ml NuPAGE™ Transfer Buffer (20×), methanol 200 ml, 1 ml antioxidant (*Invitrogen*, *ThermoFisher*), MilliQ water up to 1L); 1 % Fisher BioReagents™ Bovine Serum Albumin Protease-free Powder (*ThermoFisher*); TTBS washing buffer (*Cayman chemical*), AP (alkaline phosphatase) buffer (Tris, NaCl, $MgAc_2$, pH 9.5), p-Nitro-Blue tetrazolium chloride (50 mg/mL in 70% dimethylformamide (DMF) H_2O solution) substrate (*Europa Biosite*), 5-bromo-4-chloro-3-indolyl phosphate (BCIP) substrate (50 mg/ml in DMF); Full-length human PKN3 [1-889 amino acids of accession number NP_037487.2] was co-expressed as an N-terminal GST-fusion protein (127 kDa) with CDC37 and HSP90a using baculovirus expression system (*Carna Biosciences*); Ready-to-use BLUeye Prestained Protein Ladder (*Sigma-Aldrich*), Ready-to-use PageRuler™ Prestained Protein Ladder (*Thermo Fisher Scientific*); MOPS SDS Running Buffer (20×) (*Invitrogen, ThermoFisher*);

Multi-mode microplate reader Synergy NEO (*BioTek*); 5% Na_2CO_3 (*Sigma-Aldrich*); 0.1 N NaOH (*Appli-Chem*); 1% $K_2C_4H_4O_6$; 0.5 % $CuSO_4$ * $5H_2O$ (*BioTop*), Folin & Ciocalteu's phenol reagent (*SIGMA Life Sciences*).

2.2 METHODS

2.2.1 Amplification and Collection of Recombinant Baculovirus (MultiBac System)

Baculovirus bacmid DNA was transfected into an Sf9 insect cell monolayer using Lipofectamine LTX with PLUS reagent. The culture was monitored for 3-5 days to detect signs of infection (cell size increase and cell detachment). The supernatant containing recombinant baculovirus Passage 0 (P0) was transferred to 10 mL of log-phase Sf9 cell suspension at a density of 1.5×10^6 cells/ml. The cells were harvested after 3-5 days of infection, when Sf9 cell viability decreased to 30-40%. The P1 viral supernatant was clarified by centrifugation at 2300 × g for 10 minutes and filtered through low protein-binding PES syringe filters (0.22 µm) and stored at 4 °C in light-protected tubes or for long-term storage at -80 °C (Allikalt et al., 2024). The viral stock was further amplified to obtain a high-titer P2 stock.

2.2.2 Image-Based Cell-Size Estimation (ICSE) Assay for Baculovirus Quantification

Sf9 cells were diluted to the following concentration: 8×10^5 cells/ml. Three-fold serial dilutions of the baculovirus stock were prepared; with one sample serving as a control in serum-free insect cell growth medium. 250 µl of Sf9 cell suspension was added to each well of a 24-well plate, followed by incubation at 27 °C for 20–30 min. Then, 250 µl of each virus dilution was added; medium without baculovirus was included as a negative control. Cell diameters were measured after a 24h of incubation. The Cytation 5 imaging microplate reader with Gen6 software was used for imaging. Imaging was performed in the brightfield mode using a UPLFLN 4× objective lens (WD 17, NA 0.13) (*Olympus, Waltham, MA*). Four images were taken from each well, each positioned 2000 µm away from the well center due to an uneven cell distribution at the well centre. Cell diameters in the images were measured using ICSE-Tools software (Laasfeld et al., 2017).

The titer was calculated by fitting the relationship between cell diameter and sample dilution factor. For this, a three-parameter function was used (GraphPad Prism 5).

Functions derived from (Equation 1), where D is the measured mean cell diameter, D_{unif} is the diameter of uninfected cells, D_{inf} is the diameter of infected cells, x is the dilution factor of the baculovirus sample used, and Z is a function of the dilution factor of the baculovirus sample that predicts the fraction of infected cells.

$$D(x) = D_{unif} + (D_{inf} - D_{unif}) \times Z(x) \quad (1)$$

If one baculovirus particle infects one cell, the following function can be used (Equation 2), EC_{50} represents the reciprocal of the dilution factor at which 50% infection is achieved.

$$Z(x) = \frac{1}{1 + 10^{logEC_{50} - log(x)}} \quad (2)$$

Considering the number of cells per well (2×10^6), the baculovirus concentration can be calculated and expressed as infectious particles per milliliter (ivp/ml).

2.2.3 Expression of hPKN3 and hPKN3 with PDPK1 via Baculovirus expression system

Expression of recombinant hPKN3 and hPKN3 co-expressed with PDPK1 was performed in Sf9 insect cells. The cells were maintained at 27 °C in EX-CELL® 420 serum-free insect cell growth medium. The volume of baculovirus required to infect the Sf9 culture was calculated using the following formula:

$$Volume\ of\ Virus\ (ml) = Desired\ MOI \times Number\ of\ cells / Virus\ Titer\ (ivp/ml)$$

150-180 ml of Sf9 cell suspension at density of 2×10^6 cells/ml was infected with high titer of rBV1, rBV2 and rBV3 (as control) viruses at MOI ≈ of 0.17–0.19. Sf9 cells were collected when viability reached 80% after 50-70 hours after infection. The cells were centrifuged at 2300× g for 10 minutes. The cell pellets were stored at -80°C. We have collected the cell pellets from 150 ml of Sf9 cells expressing hPKN3 and 160 ml of Sf9 cells expressing hPKN3×PDPK1 or control cells.

2.2.4 Lysis of Sf9 cells

Cell pellets were washed with DPBS and centrifuged at 2000× g for 5 minutes at 4 ℃. Cells were lysed in lysis buffer at a ratio of 1 ml per 10 million cells. The lysis buffer was prepared and kept on ice, as well as all reagents for the lysis buffer (1% Triton X, 50 mM Tris-HCl, 150 mM NaCl, 10 mM glycerol-2-phosphate, 0.5 mM DTT, Phosphatase Inhibitor Cocktail, Protease Inhibitor Cocktail, except the solutions dissolved in dimethyl sulfoxide and DPBS. DTT and Phosphatase/Protease Inhibitor Cocktails were added last. The lysis buffer was added to the cell pellet and incubated for an hour (vortexed every 15 minutes). After incubation, the lysate was centrifuged at maximum speed for 20 minutes at 4℃. The lysate was kept at –20 ℃ prior to use.

2.2.5 Affinity chromatography Using Strep-Tactin® Superflow® High-Capacity Resin

Affinity chromatography was performed at 4 °C in a cold room. The Strep-Tactin® column, which was prepacked with Strep-Tactin® Superflow® high-capacity resin, was equilibrated with Buffer W. The sample was loaded onto the column and allowed to flow through by gravity flow, and the flow-through fraction was collected. Next, five wash fractions of 1 column volume (CV) each, were collected with Buffer W. The target protein was eluted with Buffer E, and six fractions of 0.5 CV were collected. The column was regenerated using 1 CV of Buffer R according to the manufacturer's instructions (*IBA Lifesciences*).

2.2.6 Western Blot Analysis

The samples were mixed with a loading buffer at a 3:1 ratio and heated at 70 °C in a thermomixer. The running gel was prepared (30% acrylamide, 0.8% bis-acrylamide; 4 x Tris/SDS pH 8.8; Milli-Q water; 10% APS; 10 µL of TEMED), and the stacking gel was prepared (30% acrylamide, 0.8% bis-acrylamide; Tris/SDS pH 6.8; Milli-Q water; 10% APS; 4 µL of TEMED). Each gel was polymerized for 20 min. SDS-PAGE was performed at 110 V, then the voltage was increased to 130 V until sufficient protein separation was achieved. The PVDF membrane was activated briefly in methanol and equilibrated in transfer buffer for 15 min. After the SDS-PAGE, proteins were transferred onto PVDF membrane by electroblotting (20 minutes at 15 V). Then, the membrane was

incubated in 1% BSA (prepared in DPBS) solution for 1 hour in a rotator shaker followed by incubation (overnight at 4 °C) with primary antibodies diluted 1:2000 in 1% BSA. The membrane was washed 3 times with TTBS buffer (brief rinse, 3 min, and 15 min washes) followed by incubation with secondary antibody diluted 1:5000 in 1% BSA and incubated for 3 hours at +4 °C. After washing three times with TTBS, the membrane was incubated in AP buffer for 30 min and subsequently treated with substrate (prepared in AP buffer) until a sufficient signal developed.

Relative phosphorylation levels were quantified based on band intensities obtained using ImageJ software, where $I(anti-phospho)$ represents the intensity of the band detected with a phospho-specific antibody and $I(anti-PKN3)$represents the intensity of the corresponding total protein band. The values were not normalised to the GST-hPKN3 control, as it does not serve as a phosphorylation control and cannot be used to assess phosphorylation status. Therefore, the results represent a comparative measure of relative Strep-hPKN3 phosphorylation between samples.

$$Relative\ phosphorylation\ = \frac{I(anti-phospho)}{I(anti-PKN3)} \tag{3}$$

2.2.7 Affinity Purification Using Magnetic Strep-Tactin® XT beads

MagStrep® Strep-Tactin® XT beads were resuspended and separated using a magnetic separator. The beads were equilibrated in Buffer W by repeated washing: the tubes were placed on a magnetic separator, the supernatant was removed, and fresh Buffer W was added. This step was performed three times. Samples were added to the equilibrated beads and gently resuspended. The bead–sample mixture was incubated overnight at 4 °C to facilitate binding of Strep-tagged proteins. Following incubation, the beads were washed three times with Buffer W. The beads were then resuspended in Buffer BXT and incubated for 30 min to elute bound proteins. The eluates were collected using a magnetic separator. The procedure was performed according to the manufacturer's protocol (*IBA Lifesciences*) with modifications, including extended incubation times during the binding and elution steps to improve immobilisation of the Strep-tagged proteins and enhance elution efficiency.

2.2.8 Fluorescence Microscopy Bead-Based Assay

Bead-immobilised samples were resuspended in DPBS and transferred to a low non-specific binding 48-well microscopy chamber . Samples were stained as follows: positive samples were incubated with a polyclonal rabbit anti-PKN3 primary antibody (1:5000 dilution), followed by an Abberior STAR RED-conjugated anti-rabbit secondary antibody (1:1000 dilution). Secondary antibody-only controls were incubated with the fluorescent secondary antibody alone, while blank controls were incubated with DPBS only.

Imaging was performed using a microscopy setup as previously described (Kopanchuk et al., 2022; Vavers et al., 2026). The system was equipped with UPLSAPO 10× (NA 0.3), 20× oil (NA 0.85), and TIRF APON 60× oil (NA 1.49) objective lenses (Olympus Corp., Tokyo, Japan). Fluorescence excitation was provided by a 638 nm (150 mW) PhoxX laser diode (Omicron Laserage, Rodgau, Germany) integrated into a SOLE-6 light engine. Illumination was controlled via a Yanus scan head and a Polytrope galvanometric mirror (Till Photonics/FEI), enabling both widefield epifluorescence and highly inclined and laminated optical sheet (HILO) imaging.

Excitation and emission light paths were separated using a filter cube containing a quad-line beamsplitter (zt405/488/561/640rpc; Chroma Technology Corp.) and a quad-line emission filter (ZET 405/488/561/640; Chroma). A brightfield channel was used to define bead boundaries. Fluorescence signals were detected using an EMCCD Ultra 897 camera (Andor Technology, Belfast, UK) equipped with a TuCam adapter providing 2× magnification. The camera was cooled to −100 °C using a recirculating chiller (Oasis 160; Solid State Cooling Systems, USA).

Z-stack fluorescence images were acquired from multiple fields of view (FOVs) (≥6 per well) at three magnifications: 10× air objective, 20× oil immersion objective, and 60× oil immersion objective. Z-stacks consisted of 100 optical sections acquired using piezo-driven focusing, with step sizes of 200, 500, or 1000 nm depending on the objective magnification. Laser power and exposure time were optimized for each objective to ensure adequate signal-to-noise ratios and were kept constant across all samples. HILO illumination was applied at 20× and 60× magnifications to reduce background fluorescence from unbound secondary antibodies.

Widefield epifluorescence Z-stacks were deconvolved using the EpiDEMIC plugin (Soulez et al., 2012) in the ICY platform. Z-stacks were processed by maximum intensity projection, and the summed fluorescence intensity per FOV was calculated. Background correction was performed by subtracting the mean signal of blank controls. Positive (sample, primary antibody and secondary antibody containing) and negative (non-specific binding - without primary antibody) populations were pooled across replicate wells and FOVs. Assay performance was evaluated using the signal-to-noise ratio (S/N), defined as the ratio of mean positive signal to mean negative signal, and the robust Z′ factor (Atmaramani et al., 2020).

The robust Z′ factor was calculated as:

$$Z'_{M} = 1 - \frac{3MADc^{+} + 3MADc^{-}}{|Mc^{+} - Mc^{-}|} \quad (4)$$

2.2.9 Lowry Protein Assay for Quantification

Reagent A consisted of 5% Na_2CO_3 and 0.1 N NaOH in Milli-Q water. Reagent B consisted of 1% $K_2C_4H_4O_6$ in Milli-Q water, and Reagent C consisted of 0.5% $CuSO_4 \cdot 5H_2O$ in Milli-Q water. Reagent E was prepared fresh by mixing 48 parts of Reagent A, 1 part of Reagent B, and 1 part of Reagent C. Calibration curves were prepared in lysis buffer, elution buffer, and DPBS using a 3:5 serial dilution series of bovine serum albumin (BSA). For protein quantification, 30 µL of each BSA standard or sample was added to a 48-well plate. Subsequently, 150 µL of Reagent E was added to each well, and the plate was immediately mixed and shaken for 10 min on a rotating shaker. Folin–Ciocalteu's phenol reagent (1:1 dilution) was then added, followed by incubation for 30 minutes in the dark. Absorbance was measured using a Synergy Neo multimode plate reader (*BioTek Instruments*). Absorbance spectra were recorded using a monochromator scan over the range of 700–800 nm with 1 nm increments. The maximum absorbance peak was observed between 740 and 750 nm and was used for quantitative analysis. Protein concentrations were determined using the corresponding calibration curve.

3 RESULTS AND DISCUSSION

hPKN3 is a serine/threonine protein kinase that is overexpressed in cancer cell lines and is therefore an attractive target for inhibitor development and for studying its regulation, activity, and substrate recognition. Since the activity of hPKN3 depends on its phosphorylation, producing phosphorylated hPKN3 is crucial for obtaining a functional form of the enzyme. The MultiBac system provides a suitable platform for producing phosphorylated PKN3 in Sf9 insect cells, as it allows co-expression of PKN3 with its upstream activating kinase, PDPK1. Following expression, Strep-Tactin affinity purification can be used to isolate hPKN3; however, conventional Strep-Tactin column purification may be limited by cost and poor column resin regeneration. Therefore, magnetic bead-based immobilisation can be explored as an alternative strategy for capturing hPKN3 on MagStrep Strep-Tactin XT beads, to establish conditions suitable for future fluorescence-based assays.

3.1 rBV1 and rBV2 Titer Determination and Recombinant Expression of hPKN3 and hPKN3 Co-expressed with PDPK1

Prior to infection, the recombinant baculoviruses rBV1 and rBV2 were amplified to obtain high-titer stocks, ensuring efficient recombinant protein expression in Sf9 cells. As shown in (Figure 4), a sigmoidal relationship was observed between Sf9 cell diameter and baculovirus dilution factor, as determined by the ICSE assay.

The plateau in cell diameter indicates that the majority of Sf9 cells were infected, demonstrating that virus amplification to passage 3 resulted in a titer sufficiently high to achieve effective infection of the Sf9 culture. This enabled the successful initiation of recombinant expression of hPKN3 both alone and co-expressed with PDPK1.

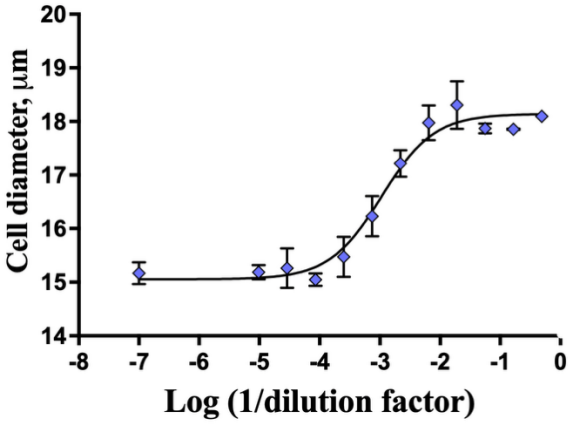

Figure 4. Titration sigmoidal curve of rBV1. The mean diameter (µm) of Sf9 cells is on the y-axis, and the negative logarithm of the virus dilution factor -log(ivp/ml) is on the x-axis. Cell diameters were measured after 24 hours of incubation using ICSE-based assay.

	rBV1	**rBV2**
$LogEC_{50}$	-2.97 ± 0.12	-2.35 ± 0.11
ivp/ml	$2.2 \cdot 10^8$	$5.5 \cdot 10^7$
R^2	0.94	0.95

Table 1. Best-fit parameters for ICSE-based baculovirus titer determination for rBV1 and rBV2. The following parameters are included: the concentration of baculovirus particles is expressed in ivp/ml; the logarithmic value ($LogEC_{50}$) of the baculovirus concentration resulting in 50% of the infection; standard error of the fitted $LogEC_{50}$ value, and the R^2 values.

3.2 Western Blot Analysis of hPKN3 and hPKN3 co-expressed with PDPK1 expression in Sf9 Insect Cells

Western blot analysis was performed to assess the expression and phosphorylation of hPKN3 co-expressed with PDPK1 and to compare it with hPKN3 expressed alone. Sf9 cells infected with empty baculovirus (rBV-empty) were used as a negative control. Total PKN3 levels were detected using an anti-PKN3 antibody.

The full-length hPKN3 has a molecular weight of approximately 99 kDa; therefore, bands observed in cell lysates between ~93 and 130 kDa were attributed to hPKN3. Recombinant GST-hPKN3 was used as a positive control and was detected at a higher

molecular weight due to the presence of the GST tag (Figure 5). Additional bands at lower molecular weights were also observed, indicating partial proteolytic degradation of the expressed proteins. This is consistent with expression under the polyhedrin and p10 promoters, which are active at late stages of baculovirus infection, when Sf9 cells experience significant stress and may undergo virus-induced lysis and proteolytic degradation (Kwiatkowska et al., 2025). Despite this, distinct bands at the expected molecular weights confirm successful expression of hPKN3 and hPKN3 co-expressed with PDPK1. A weak background signal was observed in the anti-PKN3 blot, suggesting potential non-specific binding or cross-reactivity of the antibody with endogenous Sf9 proteins.

Western blot detection using a phospho-specific antibody revealed strong bands in both hPKN3 and hPKN3 (Figure 5) co-expressed with PDPK1 at the expected molecular weight range (~93–130 kDa), indicating that both proteins are phosphorylated in Sf9 cells. The rBV-empty control showed a faint band, suggesting that the phospho-specific antibody may also recognize phosphorylated endogenous kinases in Sf9 cells, such as PKN1 (pThr774) or PKN2 (pThr816). The GST-hPKN3 control also displayed a detectable band, indicating that commercially expressed GST-hPKN3 produced in Sf9 cells is at least partially phosphorylated. This suggests the presence of endogenous serine/threonine kinases in Sf9 cells capable of phosphorylating hPKN3 in the absence of PDPK1 co-expression.

To evaluate the contribution of PDPK1 to hPKN3 phosphorylation, relative phosphorylation levels were quantified from Western blots probed with anti-PKN3 and phospho-specific antibodies. Band intensities were measured using ImageJ software, and background signal from the rBV-empty control was subtracted. Relative phosphorylation was calculated by normalizing the phospho-PKN3 signal to total PKN3 levels. hPKN3 co-expressed with PDPK1 exhibited a normalized phosphorylation value of 3.5, whereas hPKN3 expressed alone showed a value of 1.9. This corresponds to an approximately 1.8-fold increase in phosphorylation upon co-expression with PDPK1. These results indicate that PDPK1 enhances hPKN3 phosphorylation, despite the presence of endogenous kinases in Sf9 cells that may also contribute to basal phosphorylation levels.

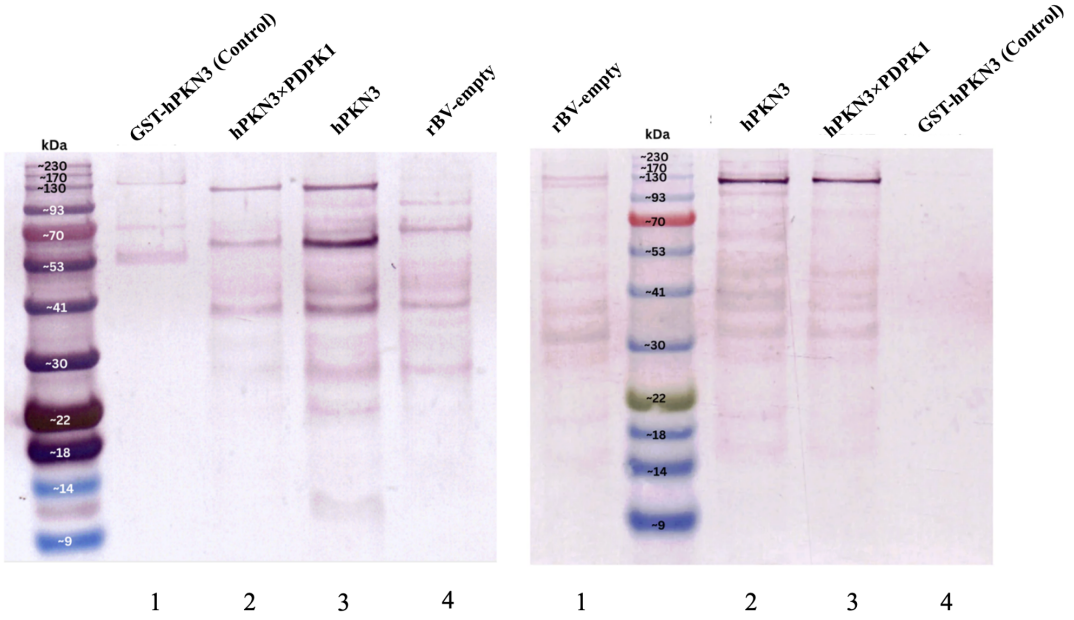

Figure 5. Western blot analysis of recombinant hPKN3 and hPKN3 co-expressed with PDPK1 in Sf9 cells. The left panel shows detection with an anti-PKN3 antibody: (1) GST-hPKN3 control, (2) hPKN3 co-expressed with PDPK1, (3) hPKN3 alone, (4) rBV-empty (negative control). The right panel shows detection with a phospho-specific antibody: (1) rBV-empty, (2) hPKN3, (3) hPKN3 co-expressed with PDPK1, (4) GST-hPKN3 control.

3.3 Western Blot Analysis following Affinity chromatography Using Strep-Tactin® Superflow® high-capacity resin

Following confirmation of hPKN3 co-expressed with PDPK1 expression, affinity chromatography purification was performed. All collected fractions were analysed by SDS-PAGE and Western blot. SDS-PAGE followed by Coomassie staining did not provide sufficient sensitivity to evaluate purification efficiency, likely due to the limited sample amount available in the pilot-scale experiment. Therefore, Western blot analysis was used for detection, as antibody-based methods with enzymatic signal amplification offer higher sensitivity. An anti-PKN3 antibody was used to detect total hPKN3 in the fractions. Analysis of the flow-through and wash fractions indicated that a substantial portion of the target protein did not bind to the column and was either present in the flow-through or removed during washing steps. Nevertheless, a small amount of hPKN3 that

co-expressed with PDPK1 was recovered in elution fractions, with the strongest signal observed in fractions 3 and 4 (Figure S2).

To assess the phosphorylation state of the eluted protein, the same fractions were probed with a phospho-specific antibody. As shown (Figure 6), hPKN3×PDPK1 was detected in elution fraction 4; however, comparison of phospho-specific and total PKN3 signals indicated that only a small fraction of the eluted protein was phosphorylated relative to the total recovered protein. One possible explanation for the low binding efficiency is interference from endogenous biotin present in Sf9 cells. Biotin binds to Strep-Tactin matrices with extremely high affinity, potentially occupying binding sites and preventing efficient interaction of the Strep-tagged protein with the resin. As the streptavidin–biotin interaction is among the strongest known non-covalent interactions, it is effectively irreversible under standard purification conditions, which can hinder regeneration of the resin. Consequently, prior exposure of the column to free biotin may reduce binding capacity in subsequent purification cycles, limiting the reusability and cost-efficiency of Strep-Tactin affinity chromatography.

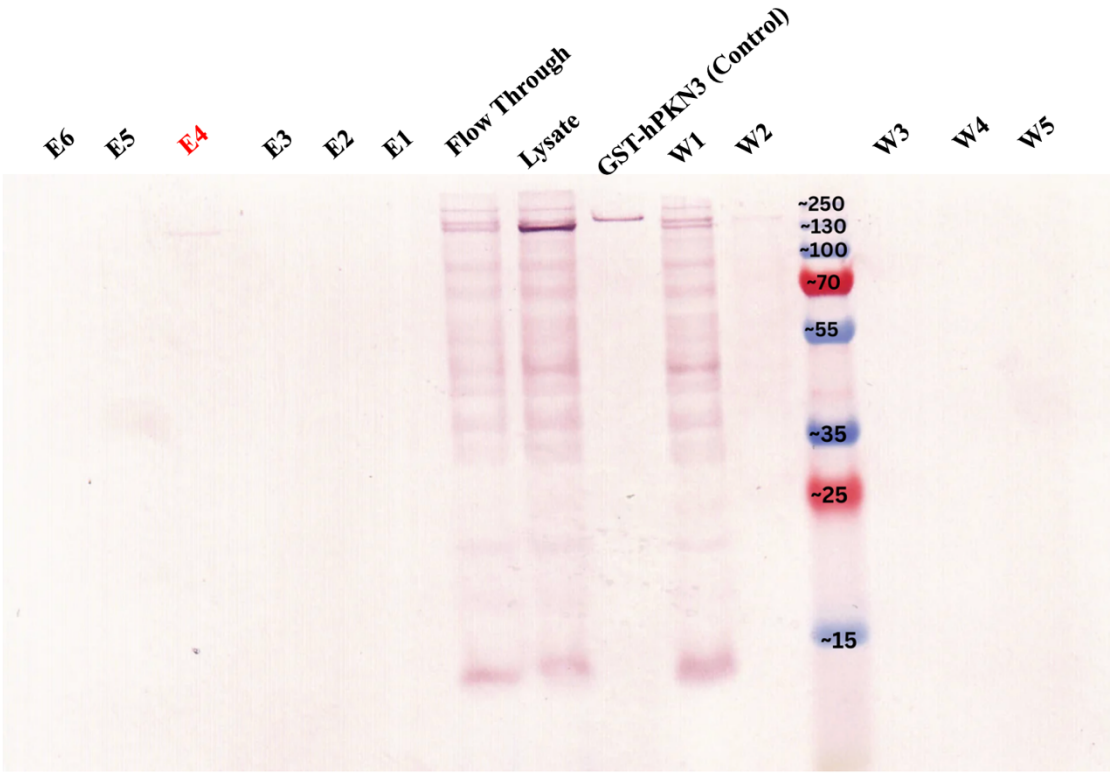

Figure 6. Western Blot detection of hPKN3×PDPK1 after Strep-Tactin® Superflow® high-capacity affinity chromatography purification. Flow-through, wash, and elution fractions were detected with phospho-specific Anti-PKN3 (pT718), PRK1 (pT774), PKN2 (pT816) antibody. The target protein was detected in elution fraction 4, though at very low level.

3.4 Evaluation of Magnetic Bead-Based Fluorescence Microscopy Assay Using MagStrep® Strep-Tactin® XT Beads

As affinity chromatography using Strep-Tactin® Superflow® high-capacity resin with desthiobiotin-containing elution buffer (2.5 mM) resulted in limited recovery of hPKN3, likely due to interference from endogenous biotin binding to the Strep-Tactin matrix, an alternative strategy was investigated. Specifically, the feasibility of capturing hPKN3 on MagStrep® Strep-Tactin® XT beads and detecting the protein in an immobilised state using fluorescence-based methods was evaluated.

In this approach, non-specifically bound proteins were removed through washing steps, while the elution step was excluded. This allowed antibody-based detection of bead-immobilised proteins. Due to the incompatibility of the phospho-specific antibody with the fluorescence-based assay, only a primary anti-PKN3 antibody was used.

Strong fluorescence signals were observed for both hPKN3 (Figure 7, panels 1A and 2A) and hPKN3 co-expressed with PDPK1 (Figure 7, panels 1C and 2C) following incubation with the primary anti-PKN3 antibody and an Abberior STAR RED-conjugated secondary antibody. This indicates successful antibody-mediated detection of the target protein immobilised on the Strep-Tactin XT bead surface via the Strep-tag.

Control experiments confirmed the specificity of the assay. Samples incubated only with the secondary antibody (Figure 7, panels 3A–3D) showed no detectable fluorescence signal, demonstrating that the observed fluorescence depends on primary antibody binding and is not due to non-specific interactions with the bead surface. Similarly, samples without any antibody addition (Figure 7, panels 1B, 2B, 1D, and 2D) showed no signal, further confirming antibody-dependent detection.

The rBV-empty control incubated with both primary and secondary antibodies (Figure 7, panels 4A and 4B) exhibited only weak background fluorescence, likely arising from minimal non-specific antibody binding. Comparable low background levels were observed for rBV-empty samples incubated with secondary antibody only (Figure 7, panel 4C), while no signal was detected in the absence of antibodies (Figure 7, panel 4D). Quantitative analysis (Figure 8) demonstrated a strong fluorescence signal in positive samples compared to negative and blank controls. The signal was calculated as summed fluorescence intensity per field of view of maximum intensity projected Z-stacks. The positive group included samples incubated with both primary and secondary antibodies, whereas the negative group contained only the secondary antibody, and the blank group without antibody treatment.

Overall, these results demonstrate that MagStrep® Strep-Tactin® XT beads provide an effective platform for capturing hPKN3 and hPKN3 co-expressed with PDPK1 and enable their detection using fluorescence microscopy. The observed signal was highly dependent on specific recognition by the primary antibody and was not significantly influenced by bead autofluorescence or non-specific binding of secondary antibodies.

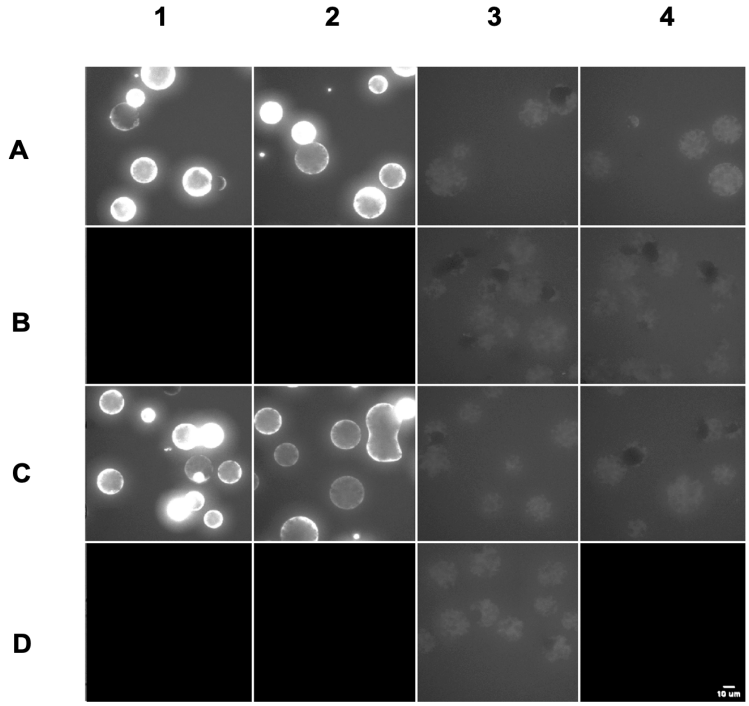

Figure 7. Fluorescence-based detection of magnetic bead-bound hPKN3 and hPKN3 co-expressed with PDPK1.

hPKN3 samples: (A1, A2) primary polyclonal rabbit anti-PKN3 antibody followed by fluorescent secondary antibody; (B1, B2) no secondary antibody control; (A3, B3) no primary antibody control.

hPKN3 co-expressed with PDPK1: (C1, C2) primary anti-PKN3 antibody followed by fluorescent secondary antibody; (D1, D2) no secondary antibody control; (C3, D3) no primary antibody control.

rBV-empty control: (A4, B4) primary and secondary antibody; (C4) no primary antibody control; (D4) no secondary antibody control.
Fluorescence imaging was performed using HILO excitation at 20× magnification.
Scale bar 10 µm.

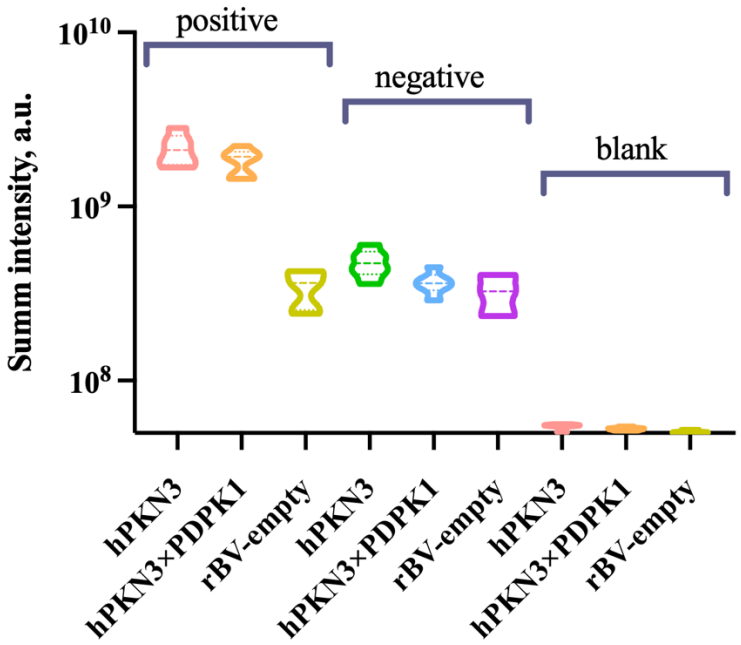

Figure 8. Comparison of fluorescence intensities of bead-immobilised hPKN3, hPKN3×PDPK1 and rBV-empty samples using HILO excitation at 60× magnification. The y-axis represents fluorescence intensity, calculated as the summed fluorescence signal per field of view. The positive sample group contained both primary anti-PKN3 antibody and fluorescent secondary antibody, the negative group contained only the secondary antibody, and the blank group contained no secondary antibodies. The strong fluorescence signal observed in the positive group indicates specific detection of immobilised PKN3 constructs mediated by the primary anti-PKN3 antibody.

3.4.1 Robust Assessment of Assay Quality

The effect of magnification on macroscopic assay performance was evaluated by analysing the signal-to-noise ratio (S/N) and robust Z′ factor. Quantitative analysis of the far-red fluorescence signal demonstrated a clear increase in S/N with increasing magnification (Table 2). For hPKN3, S/N increased from ~1.2 at 10× to ~2.1 at 20× and ~5.0 at 60×. Similarly, for hPKN3 co-expressed with PDPK1, S/N increased from ~1.35 at 10× to ~2.42 at 20× and ~5.68 at 60×. In contrast, the rBV-empty control exhibited S/N values close to unity across all magnifications, confirming that the observed signal enhancement is specific to immobilised hPKN3 constructs.

Assay performance was further assessed using the robust Z′ factor based on the median and median absolute deviation (MAD) (Table 2). For hPKN3, the highest assay quality was observed at 20× magnification (Z′ ≈ 0.73), indicating excellent separation between positive and negative sample populations. At 60× magnification, Z′ decreased to approximately 0.26, suggesting increased variability despite higher signal intensity. In contrast, hPKN3 co-expressed with PDPK1 demonstrated improved performance at higher magnification, with Z′ increasing from ~0.28 at 20× to ~0.61 at 60×, corresponding to a transition from moderate to good assay quality. The rBV-empty control exhibited negative Z′ values across all magnifications, consistent with the absence of meaningful signal separation.

Construct	Magnification	S/N ± SEM	Robust Z′
hPKN3	10×	1.21 ± 0.13	-0.81
hPKN3	20×	2.08 ± 0.15	**0.73**
hPKN3	60×	5.0 ± 0.6	**0.26**
hPKN3×PDPK1	10×	1.35 ± 0.10	-0.06
hPKN3×PDPK1	20×	2.4 ± 0.3	**0.28**
hPKN3×PDPK1	60×	5.7 ± 0.6	**0.61**
Control (rBV-empty)	10×	0.97 ± 0.02	-0.21
Control (rBV-empty)	20×	0.90 ± 0.07	-0.49
Control (rBV-empty)	60×	1.1 ± 0.3	-9.90

Table 2. Comparison of hPKN3, hPKN3×PDPK1 and rBV-empty different magnifications (10x, 20x, 60x), including their S/N ± SEM and Robust Z' values. For the Strep-hPKN3 construct, the 20x magnification showed the best assay quality based on the robust Z' value, whereas for hPKN3×PDPK1 the highest robust Z' value was observed at 60x magnification. Bold values indicate good to excellent quality.

Relative improvements in S/N with increasing magnification are summarised in Table 3. Increasing magnification from 20× to 60× resulted in more than a two-fold enhancement in S/N, while comparison between 10× and 60× magnification showed approximately four-fold improvement. These results demonstrate a strong dependence of detection sensitivity on magnification, although the associated variability differs between constructs.

Construct	60× vs 20×	60× vs 10×
hPKN3	2.4 ± 0.7	4.1 ± 1.4
hPKN3×PDPK1	2.3 ± 0.7	4.2 ± 1.1

Table 3. Comparison of relative improvements in S/N ration with increasing magnification for hPKN3 and hPKN3×PDPK1 fluorescence imaging. Values represent fold-change in S/N at 60× magnification relative to 20× and 10× magnifications

Overall, increasing magnification enhances fluorescence signal intensity and S/N; however, its impact on assay quality depends on the balance between signal separation and variability. For hPKN3, optimal assay performance was achieved at 20× magnification, where Z′ reached ~0.73, indicating excellent assay quality. Although the signal intensity at 60× was substantially higher, increased variability reduced the Z′ factor. In contrast, hPKN3 co-expressed with PDPK1 showed improved Z′ at higher magnification (Z′ ≈ 0.61 at 60×), indicating that the stronger signal outweighed the increase in variability.

These differences are influenced by the imaging configuration. The 10× air objective does not support HILO illumination, resulting in elevated background fluorescence and reduced contrast. In contrast, both 20× and 60× oil immersion objectives enable HILO excitation, which suppresses out-of-focus fluorescence and significantly improves contrast. This leads to increased S/N and improved assay performance at higher magnifications.

Differences in Z′ between constructs further suggest that variability at high magnification is influenced by signal distribution and sampling effects. At 60× magnification, the number of beads per field of view is reduced, increasing sensitivity to local fluctuations in signal intensity. For hPKN3, this results in increased variability and reduced assay robustness. However, for hPKN3 co-expressed with PDPK1, the stronger fluorescence signal compensates for this effect, leading to improved assay performance.

These findings highlight that assay optimisation requires balancing optical sensitivity with statistical robustness. While higher magnification increases signal intensity, it does not uniformly improve assay quality and depends on both the biological system and imaging conditions.

The strong separation achieved at 20× magnification demonstrates that this configuration is well-suited for quantitative fluorescence assays of immobilised proteins. The system shows strong potential for future applications, including ligand-binding studies and inhibitor screening directly on bead-immobilised hPKN3.

Although 60× imaging provides higher sensitivity, its performance is currently limited by sampling constraints. This limitation is not intrinsic to the optical system but is related to bead size and experimental design. Performance at higher magnification could be improved by reducing bead size to increase the number of beads per field of view, increasing the number of analysed fields (at the expense of acquisition time), averaging multiple Z-stacks or deconvolution outputs, and applying segmentation-based image analysis approaches. Brightfield contrast provides a suitable basis for such segmentation. These improvements would allow the enhanced sensitivity of high-magnification imaging to be fully exploited without compromising assay robustness.

3.4.2 Elution of hPKN3 from MagStrep® Strep-Tactin® XT beads

To address the limited assay performance observed at 10× magnification in the initial analysis (where segmentation was not applied), a dedicated image analysis workflow was developed. This workflow incorporated automated preprocessing, robust bead segmentation using hierarchical k-means clustering, and quantitative fluorescence extraction normalised to bead area. This approach enabled reliable signal analysis even at low magnification.

Application of the segmentation-based workflow significantly improved the analytical performance of the 10× dataset. In contrast to the initial analysis, in which 10× imaging yielded poor assay quality, the refined pipeline enabled effective discrimination between positive and negative populations, resulting in a robust Z' factor of 0.55. This indicates good assay quality and reliable separation of signal from background. These results demonstrate that the primary limitation of the 10× configuration was not solely due to optical sensitivity but rather insufficient image analysis, which has now been resolved.

Importantly, the improved analysis demonstrates that bead-immobilised hPKN3 can be efficiently eluted upon addition of biotin (Figure 9). Following biotin treatment, the fluorescence signal decreased to levels comparable to non-specific binding controls,

indicating near-complete release of hPKN3 from the bead surface. This confirms that the interaction between Strep-tagged hPKN3 and Strep-Tactin beads is reversible under these conditions (Figure S3).

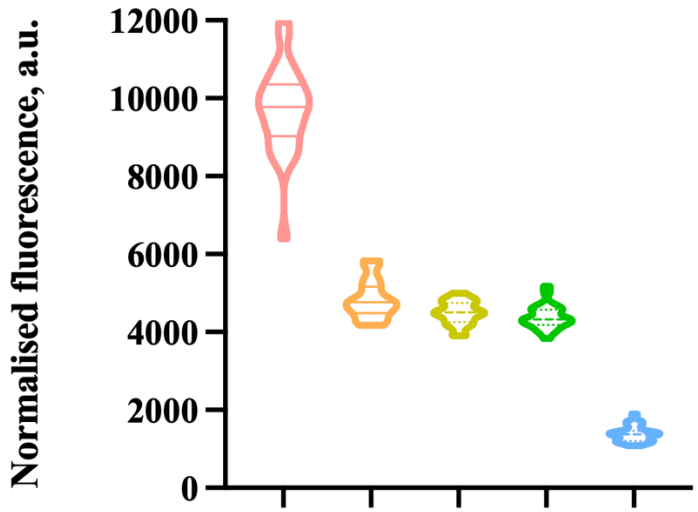

Primary antibody	+	+	-	-	+
Secondary antibody	+	+	+	+	-
Biotin	-	+	-	+	-

Figure 9. Fluorescence-based detection of bead-immobilised hPKN3 under biotin treatment. Samples were imaged using HILO excitation at 60× magnification, and fluorescence intensity is presented as normalised summed intensity per field of view. The conditions included combinations of primary anti-PKN3 antibody, fluorescent secondary antibody, and biotin. The highest fluorescence signal was observed in samples containing both primary and secondary antibodies, confirming specific detection of immobilised hPKN3. Addition of biotin reduced the signal to levels comparable to secondary antibody controls, demonstrating efficient elution of hPKN3 from the bead surface.

Quantification of hPKN3 and hPKN3 co-expressed with PDPK1 was initially attempted using the Bradford assay; however, this approach was incompatible with the composition of the lysis and elution buffers. Therefore, the Lowry protein assay was employed for protein quantification.

Three calibration curves were prepared using bovine serum albumin (BSA) standards in elution buffer, DPBS, and lysis buffer. The lysis buffer produced precipitation upon reaction with the Lowry reagent, preventing reliable absorbance measurements. In contrast, the elution buffer was fully compatible with the assay,

enabling quantification of protein in eluate fractions obtained after MagStrep Strep-Tactin XT beads purification (Figure 10). Reliable quantification was only feasible for hPKN3 eluates, as samples obtained from hPKN3 co-expressed with PDPK1 were close to the lower detection limit of the assay. The concentration of hPKN3 was determined using a standard calibration curve generated in elution buffer. When scaled to 1 L of Sf9 culture, the yield of eluted hPKN3 was estimated to be approximately 0.5 mg.

These results indicate that purification using MagStrep Strep-Tactin XT beads enables recovery of hPKN3, although the overall yield remains relatively low. While protein isolation was not the primary aim of this assay, the results demonstrate that magnetic bead-based purification is compatible with downstream fluorescence-based analysis and can support recovery of sufficient protein for analytical applications.

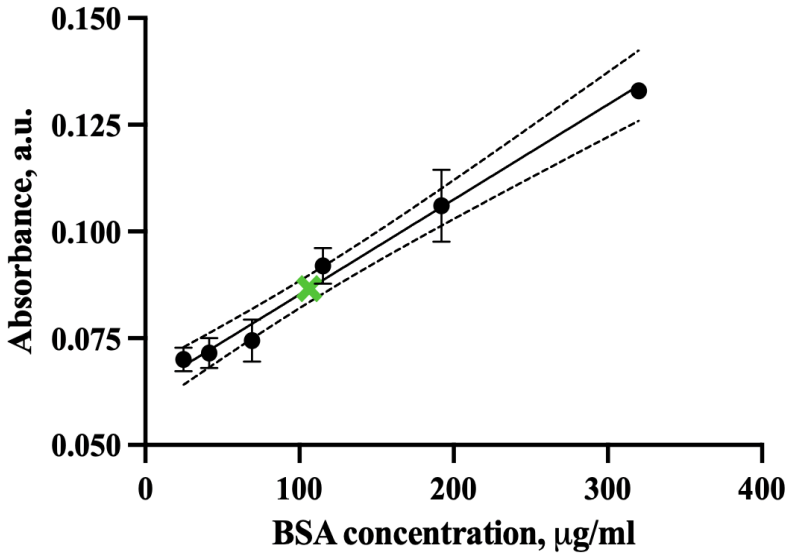

Figure 10. Lowry protein assay calibration curve prepared in elution buffer for quantification of hPKN3 eluate. BSA standards were prepared as a 3:5 serial dilution and measured following the Lowry assay. Absorbance values were plotted against protein concentration, and a linear regression model was used to determine the concentration of hPKN3 in eluate samples. The absorbance value corresponding to the hPKN3 eluate sample is indicated on the calibration curve by a green cross.

SUMMARY

In this study, human PKN3 (hPKN3) was successfully co-expressed with its upstream activator PDPK1 using the baculovirus expression system in Sf9 insect cells. Western blot analysis confirmed that co-expression with PDPK1 increases hPKN3 phosphorylation approximately 1.8-fold compared to hPKN3 expressed alone, while also revealing basal phosphorylation likely arising from endogenous kinases present in Sf9 cells.

Initial purification using Strep-Tactin affinity chromatography demonstrated limited efficiency, likely due to interference from endogenous biotin and low recovery of phosphorylated hPKN3. To overcome these limitations, a magnetic bead-based immobilisation strategy was developed and combined with fluorescence-based detection. This study demonstrates that fluorescence-based detection of immobilised hPKN3 on Strep-Tactin magnetic beads is highly sensitive and dependent on imaging configuration. Increasing magnification significantly improves signal-to-noise ratio; however, overall assay quality depends on the balance between signal intensity and variability. The 20× objective provided optimal assay performance for hPKN3 ($Z' \approx 0.73$). Importantly, the development of a segmentation-based image analysis workflow enabled reliable quantification even at low magnification (10×), where a robust Z' factor of ~0.55 was achieved. This demonstrates that analytical limitations at low magnification can be overcome through advanced image processing, enabling higher-throughput analysis without compromising assay quality. Biotin-mediated elution experiments confirmed the reversibility of Strep-tag binding, and Lowry-based quantification demonstrated that hPKN3 can be recovered following bead-based purification, though at modest yields.

Overall, this work establishes a combined biochemical and fluorescence imaging platform for analysing phosphorylated hPKN3 in an immobilised format. The system shows strong potential for quantitative applications such as ligand-binding studies and inhibitor screening, providing a foundation for future high-throughput assays targeting PKN3.

REFERENCES

Adams, J. A. (2001). Kinetic and Catalytic Mechanisms of Protein Kinases. *Chemical Reviews*, *101*(8), 2271–2290. https://doi.org/10.1021/cr000230w

Allikalt, A., Veiksina, S., Tahk, M.-J., Vavers, E., Laaneväli, E., Rinken, A., & Kopanchuk, S. (2024). MultiBacMam Technology for Studying the Downstream cAMP Signaling Pathway of M2 Muscarinic Acetylcholine Receptor. In J. Myslivecek & J. Jakubik (Eds.), *Muscarinic Receptor* (Vol. 211, pp. 153–175). Springer US. https://doi.org/10.1007/978-1-0716-4015-9_7

Ardito, F., Giuliani, M., Perrone, D., Troiano, G., & Muzio, L. L. (2017). The crucial role of protein phosphorylation in cell signaling and its use as targeted therapy (Review). *International Journal of Molecular Medicine*, *40*(2), 271–280. https://doi.org/10.3892/ijmm.2017.3036

Atmaramani, R., Pancrazio, J. J., & Black, B. J. (2020). Adaptation of robust Z' factor for assay quality assessment in microelectrode array based screening using adult dorsal root ganglion neurons. *Journal of Neuroscience Methods*, *339*, 108699. https://doi.org/10.1016/j.jneumeth.2020.108699

Beygmoradi, A., Homaei, A., Hemmati, R., & Fernandes, P. (2023). Recombinant protein expression: Challenges in production and folding related matters. *International Journal of Biological Macromolecules*, *233*, 123407. https://doi.org/10.1016/j.ijbiomac.2023.123407

Bieniossek, C., Imasaki, T., Takagi, Y., & Berger, I. (2012). MultiBac: Expanding the research toolbox for multiprotein complexes. *Trends in Biochemical Sciences*, *37*(2), 49–57. https://doi.org/10.1016/j.tibs.2011.10.005

Collazos, A., Michael, N., Whelan, R. D. H., Kelly, G., Mellor, H., Pang, L. C. H., Totty, N., & Parker, P. J. (2011). Site recognition and substrate screens for PKN

family proteins. *Biochemical Journal*, *438*(3), 535–543. https://doi.org/10.1042/BJ20110521

Di Blasio, L., Gagliardi, P., Puliafito, A., & Primo, L. (2017). Serine/Threonine Kinase 3-Phosphoinositide-Dependent Protein Kinase-1 (PDK1) as a Key Regulator of Cell Migration and Cancer Dissemination. *Cancers*, *9*(3), 25. https://doi.org/10.3390/cancers9030025

Dibus, M., Brábek, J., & Rösel, D. (2020). A Screen for PKN3 Substrates Reveals an Activating Phosphorylation of ARHGAP18. *International Journal of Molecular Sciences*, *21*(20), 7769. https://doi.org/10.3390/ijms21207769

Dundas, C. M., Demonte, D., & Park, S. (2013). Streptavidin–biotin technology: Improvements and innovations in chemical and biological applications. *Applied Microbiology and Biotechnology*, *97*(21), 9343–9353. https://doi.org/10.1007/s00253-013-5232-z

Dutta, S., Bose, K. (2022). Protein Purification by Affinity Chromatography. In: Bose, K. (eds) Textbook on Cloning, Expression and Purification of Recombinant Proteins. *Springer, Singapore*. https://doi.org/10.1007/978-981-16-4987-5_6

Falasca, M., & Fyffe, C. (2013). 3-Phosphoinositide-dependent protein kinase-1 as an emerging target in the management of breast cancer. *Cancer Management and Research*, 271. https://doi.org/10.2147/CMAR.S35026

Falk, M. D., Liu, W., Bolaños, B., Unsal-Kacmaz, K., Klippel, A., Grant, S., Brooun, A., & Timofeevski, S. (2014). Enzyme kinetics and distinct modulation of the protein kinase N family of kinases by lipid activators and small molecule inhibitors. *Bioscience Reports*, *34*(2), e00097. https://doi.org/10.1042/BSR20140010

Flynn, P., Mellor, H., Casamassima, A., & Parker, P. J. (2000). Rho GTPase Control of Protein Kinase C-related Protein Kinase Activation by 3-Phosphoinositide-dependent Protein Kinase. *Journal of Biological Chemistry*, *275*(15), 11064–11070. https://doi.org/10.1074/jbc.275.15.11064

Garcia, A. V., Al-Yousif, M., & Hirt, H. (2012). Role of AGC kinases in plant growth and stress responses. *Cellular and Molecular Life Sciences*, *69*(19), 3259–3267. https://doi.org/10.1007/s00018-012-1093-3

Gemperle, J., Dibus, M., Koudelková, L., Rosel, D., & Brábek, J. (2019). The interaction of p130Cas with PKN 3 promotes malignant growth. *Molecular Oncology*, *13*(2), 264–289. https://doi.org/10.1002/1878-0261.12401

Geneva Biotech. (2024). MultiBac^{TM}: Multi-protein expression in insect cells User manual (Version 9.0).

Johnson, J. L., Yaron, T. M., Huntsman, E. M., Kerelsky, A., Song, J., Regev, A., Lin, T.-Y., Liberatore, K., Cizin, D. M., Cohen, B. M., Vasan, N., Ma, Y., Krismer, K., Robles, J. T., Van De Kooij, B., Van Vlimmeren, A. E., Andrée-Busch, N., Käufer, N. F., Dorovkov, M. V., … Cantley, L. C. (2023). An atlas of substrate specificities for the human serine/threonine kinome. *Nature*, *613*(7945), 759–766. https://doi.org/10.1038/s41586-022-05575-3

Johnson, L. N., & Lewis, R. J. (2001). Structural Basis for Control by Phosphorylation. *Chemical Reviews*, *101*(8), 2209–2242. https://doi.org/10.1021/cr000225s

Jumper, J., Evans, R., Pritzel, A., Green, T., Figurnov, M., Ronneberger, O., Tunyasuvunakool, K., Bates, R., Žídek, A., Potapenko, A., Bridgland, A., Meyer, C., Kohl, S. A. A., Ballard, A. J., Cowie, A., Romera-Paredes, B., Nikolov, S., Jain, R., Adler, J., … Hassabis, D. (2021). Highly accurate protein

structure prediction with AlphaFold. *Nature*, *596*(7873), 583–589. https://doi.org/10.1038/s41586-021-03819-2

Kang, J.-H. (2014). Protein Kinase C (PKC) Isozymes and Cancer. *New Journal of Science*, *2014*, 1–36. https://doi.org/10.1155/2014/231418

Kopanchuk, S., Vavers, E., Veiksina, S., Ligi, K., Zvejniece, L., Dambrova, M., & Rinken, A. (2022). Intracellular dynamics of the Sigma-1 receptor observed with super-resolution imaging microscopy. *PLOS ONE*, *17*(5), e0268563. https://doi.org/10.1371/journal.pone.0268563

Kwiatkowska, J., Stein, E., Romanenko, A., Plens-Gałąska, M., Podsiadła-Białoskórska, M., Szołajska, E., Kühn, U., & Kamieniarz-Gdula, K. (2025). A beginners guide to Sf9 and Sf21 insect cell line culture and troubleshooting. *Scientific Reports*, *15*(1), 19907. https://doi.org/10.1038/s41598-025-99812-0

Laasfeld, T., Kopanchuk, S., & Rinken, A. (2017). Image-Based Cell-Size Estimation for Baculovirus Quantification. *BioTechniques*, *63*(4), 161–168. https://doi.org/10.2144/000114595

Leroux, A. E., Schulze, J. O., & Biondi, R. M. (2018). AGC kinases, mechanisms of regulation and innovative drug development. *Seminars in Cancer Biology*, *48*, 1–17. https://doi.org/10.1016/j.semcancer.2017.05.011

Pearce, L. R., Komander, D., & Alessi, D. R. (2010). The nuts and bolts of AGC protein kinases. *Nature Reviews Molecular Cell Biology*, *11*(1), 9–22. https://doi.org/10.1038/nrm2822

Quétier, I., Marshall, J. J. T., Spencer-Dene, B., Lachmann, S., Casamassima, A., Franco, C., Escuin, S., Worrall, J. T., Baskaran, P., Rajeeve, V., Howell, M., Copp, A. J., Stamp, G., Rosewell, I., Cutillas, P., Gerhardt, H., Parker, P. J., &

Cameron, A. J. M. (2016). Knockout of the PKN Family of Rho Effector Kinases Reveals a Non-redundant Role for PKN2 in Developmental Mesoderm Expansion. *Cell Reports*, *14*(3), 440–448. https://doi.org/10.1016/j.celrep.2015.12.049

Reinecke, M., Brear, P., Vornholz, L., Berger, B.-T., Seefried, F., Wilhelm, S., Samaras, P., Gyenis, L., Litchfield, D. W., Médard, G., Müller, S., Ruland, J., Hyvönen, M., Wilhelm, M., & Kuster, B. (2024). Chemical proteomics reveals the target landscape of 1,000 kinase inhibitors. *Nature Chemical Biology*, *20*(5), 577–585. https://doi.org/10.1038/s41589-023-01459-3

Roskoski, R. (2026). Properties of FDA-approved small molecule protein kinase inhibitors: A 2026 update. *Pharmacological Research*, *224*, 108107. https://doi.org/10.1016/j.phrs.2026.108107

Sahdev, S., Khattar, S. K., & Saini, K. S. (2007). Production of active eukaryotic proteins through bacterial expression systems: A review of the existing biotechnology strategies. *Molecular and Cellular Biochemistry*, *307*(1–2), 249–264. https://doi.org/10.1007/s11010-007-9603-6

Saraswat, M., Musante, L., Ravidá, A., Shortt, B., Byrne, B., & Holthofer, H. (2013). Preparative Purification of Recombinant Proteins: Current Status and Future Trends. *BioMed Research International*, *2013*, 1–18. https://doi.org/10.1155/2013/312709

Schmidt, S. R., Schweikart, F., & Andersson, M. E. (2007). Current methods for phosphoprotein isolation and enrichment. *Journal of Chromatography B*, *849*(1–2), 154–162. https://doi.org/10.1016/j.jchromb.2006.09.016

Shiga, K., Takayama, K., Futaki, S., Hutti, J. E., Cantley, L. C., Ueki, K., Ono, Y., & Mukai, H. (2010). Development of an intracellularly acting inhibitory peptide selective for PKN. *Biochemical Journal*, *425*(2), 445–543. https://doi.org/10.1042/BJ20090380

Shrestha, A., Hamilton, G., O'Neill, E., Knapp, S., & Elkins, J. M. (2012). Analysis of conditions affecting auto-phosphorylation of human kinases during expression in bacteria. *Protein Expression and Purification*, *81*(1), 136–143. https://doi.org/10.1016/j.pep.2011.09.012

Skerra, A., & Schmidt, T. G. M. (1999). Applications of a peptide ligand for streptavidin: The Strep-tag. *Biomolecular Engineering*, *16*(1–4), 79–86. https://doi.org/10.1016/S1050-3862(99)00033-9

Slovakova, M., & Bilkova, Z. (2021). Contemporary Enzyme-Based Methods for Recombinant Proteins In Vitro Phosphorylation. *Catalysts*, *11*(8), 1007. https://doi.org/10.3390/catal11081007

Smorodina, V., Jääger, E. L., Sõrmus, T., Flores, E. D. J. Z., Enkvist, E., Uri, A., & Viht, K. (2026). Selective Inhibitor of Protein Kinase PKN3 Generated by Conjugation of a Structurally Optimized Bumped N-(2-Aminoethyl)-8-anilinoisoquinoline-5-sulfonamide (H-9) with d-Arginine-Rich Chain. *Molecules*, *31*(4), 585. https://doi.org/10.3390/molecules31040585

Sophocleous, G., Owen, D., & Mott, H. R. (2021). The structure and function of protein kinase C-related kinases (PRKs). *Biochemical Society Transactions*, *49*(1), 217–235. https://doi.org/10.1042/BST20200466

Soulez, F., Denis, L., Tourneur, Y., & Thiebaut, E. (2012). Blind deconvolution of 3D data in wide field fluorescence microscopy. *2012 9th IEEE International*

Symposium on Biomedical Imaging (ISBI), 1735–1738. https://doi.org/10.1109/ISBI.2012.6235915

Ubersax, J. A., & Ferrell Jr, J. E. (2007). Mechanisms of specificity in protein phosphorylation. *Nature Reviews Molecular Cell Biology*, *8*(7), 530–541. https://doi.org/10.1038/nrm2203

Unsal-Kacmaz, K., Ragunathan, S., Rosfjord, E., Dann, S., Upeslacis, E., Grillo, M., Hernandez, R., Mack, F., & Klippel, A. (2012). The interaction of PKN3 with RhoC promotes malignant growth. *Molecular Oncology*, *6*(3), 284–298. https://doi.org/10.1016/j.molonc.2011.12.001

Urh, M., Simpson, D., & Zhao, K. (2009). Chapter 26 Affinity Chromatography. In *Methods in Enzymology* (Vol. 463, pp. 417–438). Elsevier. https://doi.org/10.1016/S0076-6879(09)63026-3

Varadi, M., Anyango, S., Deshpande, M., Nair, S., Natassia, C., Yordanova, G., Yuan, D., Stroe, O., Wood, G., Laydon, A., Žídek, A., Green, T., Tunyasuvunakool, K., Petersen, S., Jumper, J., Clancy, E., Green, R., Vora, A., Lutfi, M., … Velankar, S. (2022). AlphaFold Protein Structure Database: Massively expanding the structural coverage of protein-sequence space with high-accuracy models. *Nucleic Acids Research*, *50*(D1), D439–D444. https://doi.org/10.1093/nar/gkab1061

Vavers, E., Kopanchuk, S., Veiksina, S., Jonane, J., Mathur, C., Nasirova, N., Midekessa, G., & Rinken, A. (2026). Simultaneous Expression of Sigma-1 Receptor and Tetraspanins Highlights Pathways of Receptor Sorting Into Extracellular Vesicles. *Journal of Neurochemistry*, *170*(4), e70426. https://doi.org/10.1111/jnc.70426

Voss, S., & Skerra, A. (1997). Mutagenesis of a flexible loop in streptavidin leads to higher affinity for the Strep-tag II peptide and improved performance in recombinant protein purification. *Protein Engineering Design and Selection*, *10*(8), 975–982. https://doi.org/10.1093/protein/10.8.975

Wang, Z.-X., Wu, J.-L., Chen, J., & Yang, G.-J. (2025). PKN3 as a key regulator in cancer – From signaling pathways to targeted therapies. *Bioorganic Chemistry*, *163*, 108725. https://doi.org/10.1016/j.bioorg.2025.108725

Watanabe, G., Saito, Y., Madaule, P., Ishizaki, T., Fujisawa, K., Morii, N., Mukai, H., Ono, Y., Kakizuka, A., & Narumiya, S. (1996). Protein Kinase N (PKN) and PKN-Related Protein Rhophilin as Targets of Small GTPase Rho. *Science*, *271*(5249), 645–648. https://doi.org/10.1126/science.271.5249.645

Zheng, J., Trafny, E. A., Knighton, D. R., Xuong, N., Taylor, S. S., Ten Eyck, L. F., & Sowadski, J. M. (1993). 2.2 Å refined crystal structure of the catalytic subunit of cAMP-dependent protein kinase complexed with MnATP and a peptide inhibitor. *Acta Crystallographica Section D Biological Crystallography*, *49*(3), 362–365. https://doi.org/10.1107/S0907444993000423

Zheng, N., Wei, J., Wu, D., Xu, Y., & Guo, J. (2023). Master kinase PDK1 in tumorigenesis. *Biochimica et Biophysica Acta (BBA) - Reviews on Cancer*, *1878*(6), 188971. https://doi.org/10.1016/j.bbcan.2023.188971

Zheng, W., Li, G., & Li, X. (2015). Affinity purification in target identification: The specificity challenge. *Archives of Pharmacal Research*, *38*(9), 1661–1685. https://doi.org/10.1007/s12272-015-0635-2

SUPPLEMENTARY (APPENDIX)

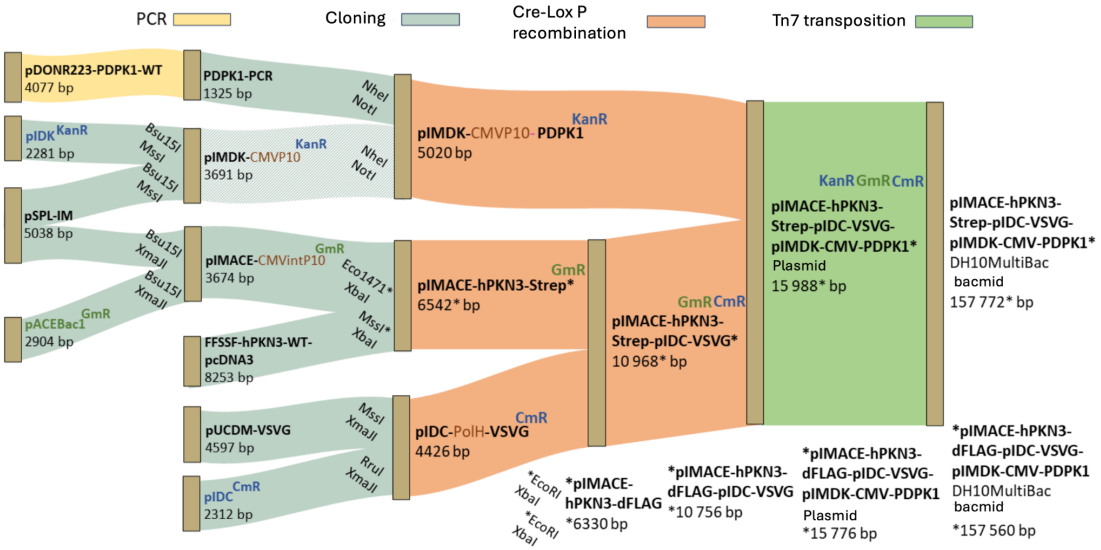

Figure S1. Schematic overview of the recombinant bacmid production. The donor plasmids are highlighted in blue and acceptor plasmids in green. Abbreviations denoting specific promoters in the plasmid names are highlighted in brown. Different background colors indicate steps (PCR, Cloning, Cre-Lox P recombination, Tn7 transposition) by which the corresponding DNA sequence was isolated or the plasmids were combined. Antibiotic resistance genes in the plasmids are indicated with superscripts. The names of the restriction enzymes used in each cloning step given in italics. (adapted from Elizabeth Undrits bachelor thesis).

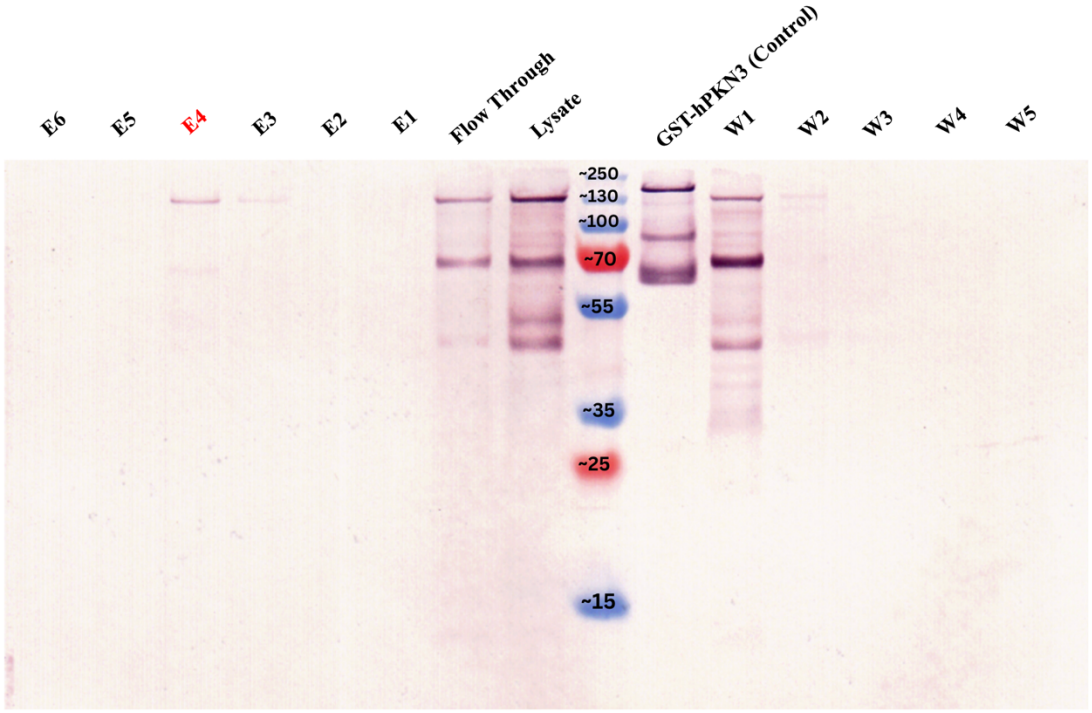

Figure S2. Western Blot Analysis performed after purification of hPKN3 co-expressed with PDPK1 with affinity Chromatography (Strep-Tactin® Superflow® high-capacity resin). Lysate, flow through, washing and elution fractions were detected with Anti-PKN3 antibody to evaluate a total content of PKN3 that can be isolated.

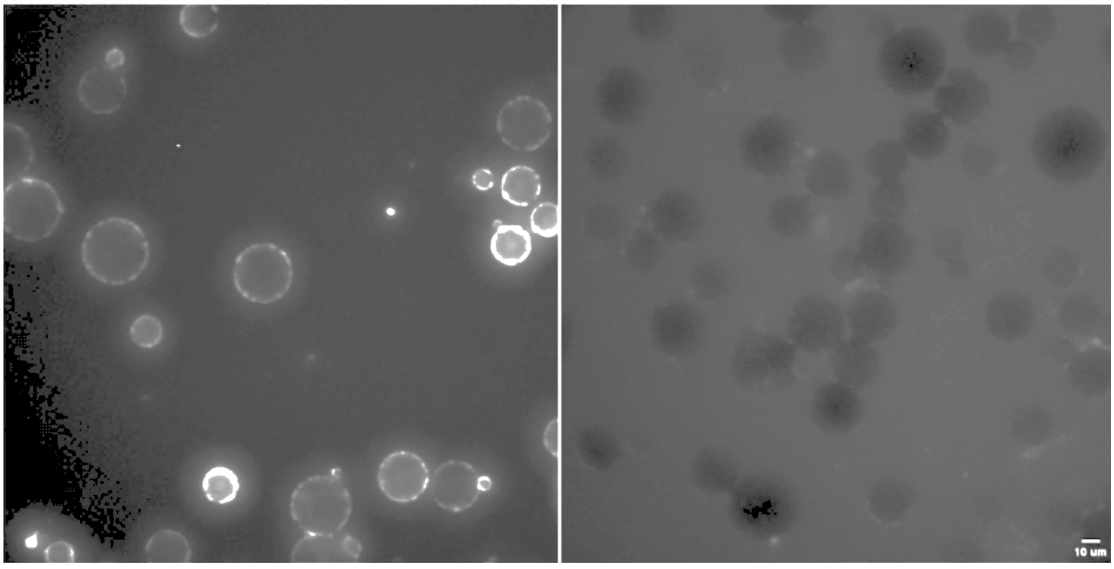

Figure S3. Fluorescence-based detection of magnetic bead-bound hPKN3 co-expressed with PDPK1 before and after biotin-mediated elution. Reduced fluorescence after biotin addition indicates that Strep-tagged hPKN3 was eluted from Strep-Tactin XT beads. Fluorescence imaging was performed using HILO excitation at 10× magnification. Scale bar 10 µm.

10x magnification objective image analysis worklow

Brightfield and fluorescence image datasets were analyzed using ICY bioimage analysis software (Institut Pasteur) with a custom protocol designed for automated batch processing.

Preprocessing and segmentation

Brightfield images were used for object detection. Files were organized by field of view, and paired brightfield and fluorescence images were matched based on identical spatial coordinates (X,Y). Pairing was performed using a custom script prior to analysis to ensure correct correspondence between channels.Before segmentation, brightfield images were preprocessed to correct for uneven illumination and to enhance bead detectability. First, uneven background gradients were corrected using Gaussian-based background subtraction. A Gaussian filter ($\sigma = 25$ pixels) was applied to the original image to generate a low-frequency background estimate. This blurred image was then subtracted from the original image, removing large-scale illumination inhomogeneity. Following background subtraction, images were intensity-inverted, converting dark bead structures into bright objects to facilitate segmentation. To further reduce local intensity variations and suppress internal bead texture, a median filter (radius 5 pixels) was applied. This step improved object homogeneity and reduced noise prior to clustering. In addition, bead structures were enhanced using spatial filtering. A band-pass filter was applied to retain structures within the expected bead size range (lower cutoff approximately half the bead radius; upper cutoff slightly larger than the bead diameter). After preprocessing, segmentation of objects (beads) was performed using the HK-means clustering algorithm, applied to the processed brightfield image. This approach enabled robust separation of beads from the background despite heterogeneous intensity distributions and internal structure. The resulting binary masks were converted into regions of interest (ROIs), corresponding to individual beads.

Measurement of fluorescence intensity

The ROIs derived from brightfield segmentation were applied directly to the corresponding fluorescence images. For each ROI, quantitative measurements were

computed using the ICY "ROI statistics" module. The following parameters were extracted for each detected object: Sum fluorescence intensity and Projected area (μm^2)

Batch processing

The analysis was performed in batch mode using ICY's protocol framework. A Python-based preprocessing step generated paired lists of brightfield and fluorescence image files, which were iterated using a range loop. For each paired dataset:

- The brightfield image was loaded and preprocessed
- Segmentation was performed using HK-means clustering
- ROIs representing individual beads were generated
- The corresponding fluorescence image was loaded
- ROI-based intensity and area measurements were calculated
- Results were exported as individual spreadsheet files for each field of view

Post-processing and normalization

Quantitative outputs from ICY were further processed in MATLAB (MathWorks). For each field of view, fluorescence intensities and areas from all detected ROIs were summed to obtain total fluorescence signal and total bead area per image. The fluorescence signal was then normalized by the corresponding total bead area, yielding an area-corrected fluorescence metric:

$$Normalized\ fluorescence = \frac{\sum Intensity}{\sum Area}$$

Custom workflow image:

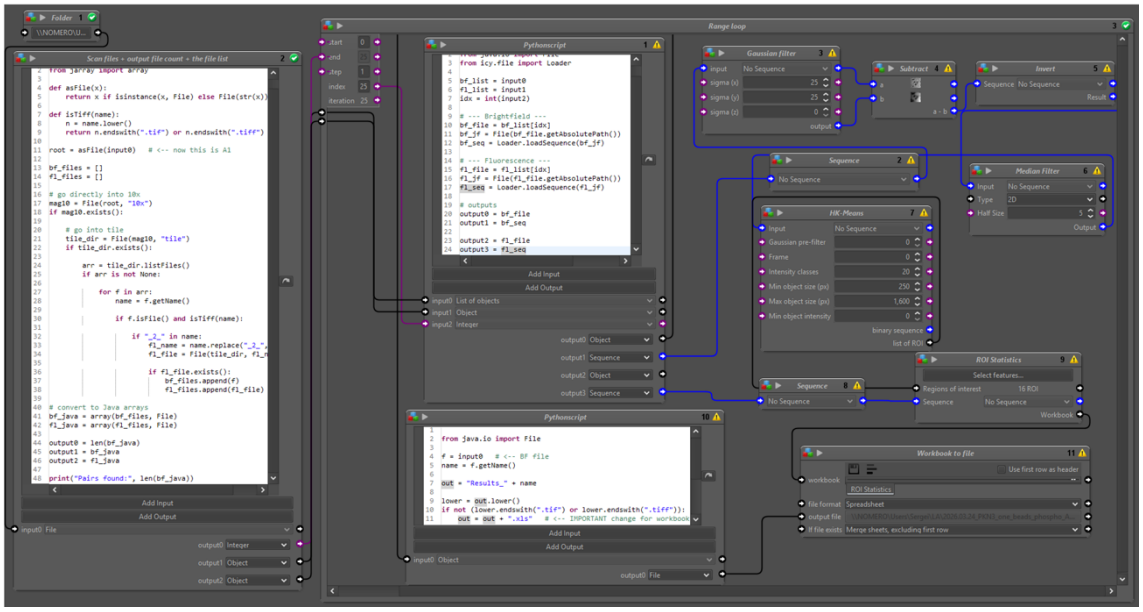

NON-EXCLUSIVE LICENCE TO REPRODUCE THESIS AND MAKE THESIS PUBLIC

I, Yelyzaveta Gushchyna,

1. grant the University of Tartu a free permit (non-exclusive licence) to

   reproduce, for the purpose of preservation, including for adding to the digital archives of the University of Tartu until the expiry of the term of copyright, my thesis:

   Establishing Phosphorylated Human Protein Kinase N3 Generation via PDPK1 Co-expression in Sf9 cells.

   Supervised by PhD Santa Veikšina, PhD Sergei Kopantšuk, PhD Kaido Viht

2. grant the University of Tartu a permit to make the thesis specified in point 1 available to the public via the web environment of the University of Tartu, including via the digital archives, under the Creative Commons licence CC BY NC ND 4.0, which allows, by giving appropriate credit to the author, to reproduce, distribute the work and communicate it to the public, and prohibits the creation of derivative works and any commercial use of the work until the expiry of the term of copyright;

3. am aware of the fact that the author retains the rights specified in points 1 and 2;

4. confirm that granting the non-exclusive licence does not infringe other persons' intellectual property rights or rights arising from the personal data protection legislation.

Yelyzaveta Gushchyna
20/05/2026